SUPERPARAMAGNETIC IRON OXIDE - ALGINATE HYDROGELS AND FLUID

This thesis is dedicated to the following teachers and the invaluable lessons they have taught me:

Victoria M. Kroll
Hard work, Honesty, Inner Strength

Melody M. Kroll
Self-worth, Determination

My Family
Love, Acceptance

Lt. Harold L. LaRock II
(U.S. Army Ranger)
Strength, Personal Achievement, Endurance

Gertle
Patience, Happiness

Nancy Lesko & Mike Quinlan
John, Irene and William Pettener
Celine Colomb-Brockman
Dr. R.F. Ziolo
and
My Canadian Sisters

SYNTHESIS AND CHARACTERIZATION OF SUPERPARAMAGNETIC IRON OXIDE - ALGINATE HYDROGELS AND FLUID

By

ELIZABETH C. KROLL, B.Sc.

A Thesis
Submitted to the School of Graduate Studies
in Partial Fulfillment of the Requirements
for the Degree
Master of Science

McMaster University

MASTER OF SCIENCE (1996) **McMASTER UNIVERSITY**

(Chemistry) **Hamilton, Ontario**

TITLE: **SYNTHESIS AND CHARACTERIZATION OF SUPERPARAMAGNETIC IRON OXIDE-ALGINATE HYDROGELS AND FLUID**

AUTHOR: **Elizabeth C. Kroll, B.Sc**
(Rochester Institute of Technology, NY, USA)

SUPERVISOR: **Dr. F. M. Winnik**

NUMBER OF PAGES: **103**

ABSTRACT

Aqueous ferrofluid has been prepared via precipitation of iron oxide into a polysaccharide gel matrix followed by degradation of the polymer to form a stable magnetic colloid. Nanocrystalline particles of iron oxide were formed in an alginate network by the alkaline hydrolysis and oxidation of the crosslinking agent, Fe^{2+}, used to bind the linear polysaccharide chains. Methanol was used to inhibit the degradation of alginate by Fe^{2+} and oxygen during the precipitation and growth of iron oxide particles. In addition, the structural integrity of the gel was maintained in part by interaction between the iron oxide particulate and the alginate matrix. Controlled chemical degradation of the matrix resulted in a aqueous suspension of alginate-stabilized magnetic iron oxide particles. The resulting fluid is orange-brown in color, optically transparent, superparamagnetic and stable between $2.8<pH<10$.

The magnetic gels were isolated as 2mm beads containing ~2-20 mmole Fe. X-ray and electron diffraction patterns of the composite correspond to maghemite (γ-Fe_2O_3) and/or magnetite (Fe_3O_4). At room temperature, the composite material is superparamagnetic with saturation magnetizations in excess of 20 emu g^{-1} at 30kOe. TEM photomicrographs of sectioned beads and of the magnetic fluid revealed the presence of spherical nanocrystalline oxide particles with diameters ranging from 3 nm to 6 nm. The iron oxide-alginate colloid has a diameter of 54nm with an average zeta potential of -51.6 mV.

ACKNOWLEDGEMENTS

I wish to thank the following people for their participation and interest in my research and for their friendship and support during my visit at McMaster University:

My friends and colleagues:

Sudarshi "Over to the right we have.." Regismond
Akiko "Angel #2" Yamazaki
Dan "How do you say...." Anghel
Vinod Pillai

and especially Leona S.K. Tomicic who bushwacked along side of me and who taught me to never walk away from a reaction.

I am also grateful for the advice and guidance of :

Gordon Hewitson
(BIMR SQUID Magnetometer)

Professor Stager
(BIMR SQUID Magnetometer, Physics Dept)

Fred Pearson and Andy Duft
(BIMR TEM Lab)

Marcie West
(Life Science TEM Lab)

Jim Britten

Brian Sayer
(McMaster NMR Facility)

Carol Dada

TABLE OF CONTENTS

Table of Contents (continued)

PAGE

LIST OF FIGURES

PAGE

List of Figures (continued)

List of Figures (continued)

PAGE

LIST OF TABLES

1. INTRODUCTION

1.1. Magnetic Nanocomposites

Nanotechnology and application-oriented materials are emerging from every discipline of science. The demand for functional nanocomposites is evidenced by the formation and growth of related industries including Nanophase Technologies, Ferrofluidics, Xerox Special Materials, and Texas NanoTech, to name a few, in addition to receiving attention and priority in government- funded programs.[1] As catalysts, alternative refrigerants [2], environmental and performance hermetic seals [3], detectable inks and toners [4], high contrast imaging agents [5], and vehicles of drug delivery, [6] solid and liquid phase magnetic products are surfacing and multiplying in both function and performance. Additionally, the synthesis of ultrafine magnetic particles has led to new advancements in the theory and understanding of small particle magnetism.

1.2. Magnetic Iron Oxides and Superparamagnetism

The magnetic properties of iron oxides and oxyhydroxides are dependent on the structure, composition and size of the oxide crystal.[7] Their magnetism arises from ions with unpaired electrons that have an associated magnetic moment. The effective magnetic moments of Fe^{2+} and Fe^{3+} are $5.4\mu_B$ and $5.9\mu_B$, respectively.[8] In a crystalline lattice, the

magnetic ions occupy regular sites depending on the crystal class. In iron minerals, interactions occur between the magnetic ions and oxygen and hydroxy ligands. This interaction influences the orientation of the electron spin within the lattice. However, the forces acting to keep electron spins ordered are opposed by thermal agitation which tends to disorder spin arrangement. The transition temperature between ordered and disordered spin configurations is specific for the type of magnetism and is an intrinsic property of all magnetic crystalline compounds. Therefore, the geometric arrangement and population of electron spins and temperature directly influence the magnetic behavior of an iron oxide or iron oxyhydroxide.

The arrangements of electron spin and magnetic moments (↑) that give rise to ferro-, antiferro-, and ferrimagnetism are shown in Figure 1.

Figure 1. Common electron spin configuration of magnetic oxides.

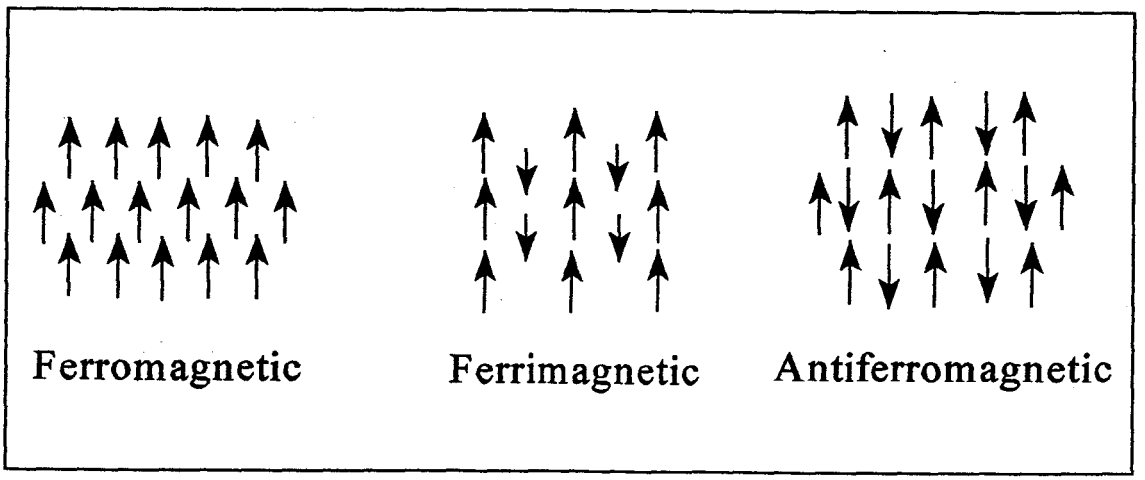

Ferromagnetism refers to electron spins which are uniformly aligned resulting in a spontaneous magnetization. Magnetism arising from an arrangement of spins which are arranged antiparallel in one sublattice and parallel in a second sublattice is termed ferrimagnetism. It is only the magnetic moments of ions, which are not cancelled by antiparallel spins, that contribute to the net magnetization of the ferrimagnet. Magnetite (Fe_3O_4), maghemite (γ-Fe_2O_3) and feroxyhyte (δ'-FeOOH) are ferrimagnets. Antiferromagnetism is a special class of ferrimagnetism in which all electron spins are arranged antiparallel. The net magnetization of antiferromagnetic solids is zero. Examples of antiferromagnetic iron oxyhydroxides and oxides include geothite (α-FeOOH), lepidocrocite (γ-FeOOH), and hematite (α-Fe_2O_3). Ferrimagnetism and antiferromagnetism are the two most common types of magnetism encountered with iron oxide minerals.

The lowest energy spin configuration of magnetic solids is a function of crystal size and shape. Single crystals and polycrystalline specimens with crystallite diameters greater then 100Å are composed of multiple magnetic domains. Domains are regions in which spins are uniformly aligned and have local magnetization. The direction of magnetization of a domain may be different than that in adjacent domains. The volume of a domain is a function of the shape of the crystalline material and the strength of an external magnetic field. The existence of domains, postulated by Neel, is the result of minimizing various energy terms contributing to the total free energy of the magnetic solid. The two main contributors are magnetic anisotropy and magnetostatic energy.[8] When the crystal size is

reduced to diameters less than 100Å, the lowest energy spin configuration is single domain, or uniform alignment of spins throughout the particle. Figure 2 shows the relationship between crystal size and domain configuration. Changes in crystal size, and subsequent spin configuration, result in different magnetic behavior.

Figure 2. Lowest energy spin configuration of multidomain and single domain crystals.

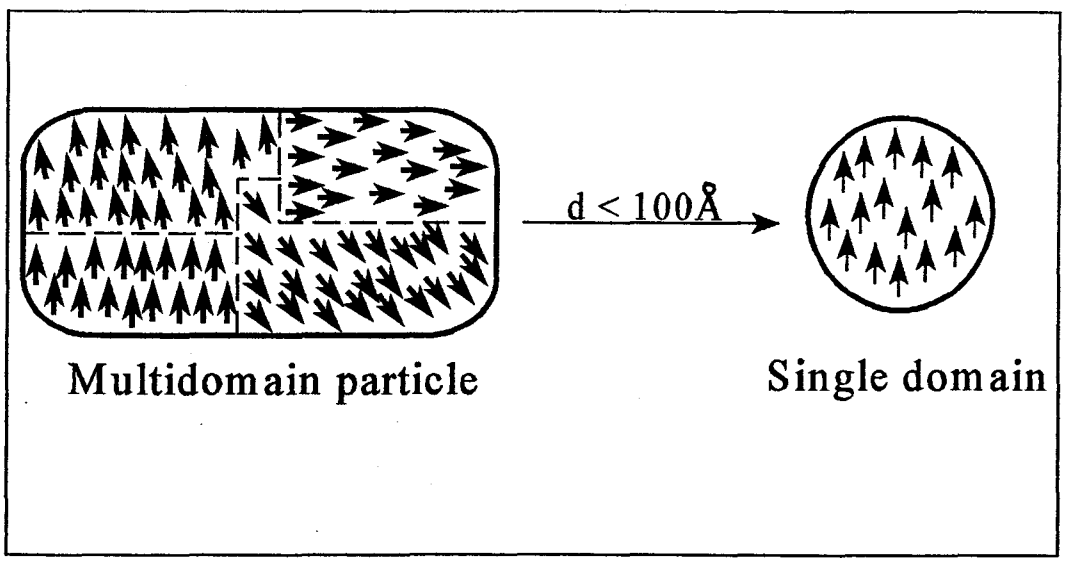

The magnetic properties of a material can be measured and represented in a magnetization curve.[9] A magnetization curve shows how the component of magnetization of a magnetic solid changes as a function of applied field strength. In Figure 3, the magnetization curves and magnetic properties characteristic of ferromagnetic

Figure 3. Magnetization curves of ferromagnetic (top) and superparamagnetic (bottom) particles

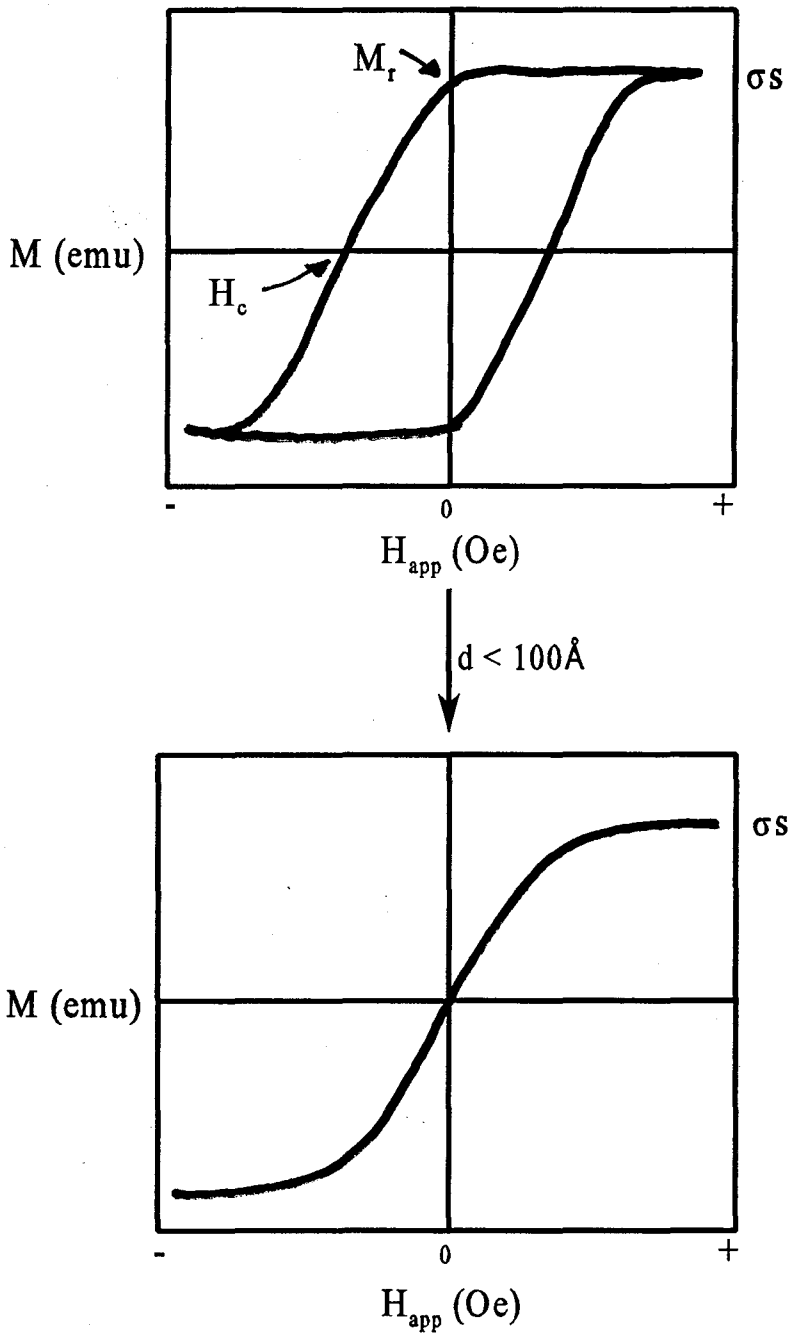

and superparamagnetic particles are shown. Initially, the ferromagnetic, multidomain particle has a net magnetization of zero in the absence of an applied field (H_{app}= 0). This is possible if the directions of magnetization of domains cancel over the entire particle. An external magnetic field is applied along a fixed axis. In weak magnetic fields, the volume of domains with spins aligned parallel with the direction of the external field expands at the expense of domains with spins oriented antiparallel. As the strength of the external field increases, the population of spins aligned with the external field increases and magnetization occurs by rotation. Saturation magnetization (σ_s) is the net component of magnetization achieved when all spins are aligned in the direction of the external field. The external field is then reduced in magnitude. When the applied field is reduced to zero (H_{app}=0), a residual magnetization from the magnetic solid exists as a result of domains remaining aligned in the direction of the absent field. The component of magnetization at zero applied field is termed remanence (Mr), or 'memory'. Coercivity (Hc) is the magnitude of external field, applied in the opposite direction, required to reduce this residual magnetization to zero. The trace of magnetization for magnetic particles is symmetric about the origin and reproducible.

Superparamagnetism is characteristic of single domain iron oxide particles and is temperature sensitive. [10] The term superparamagnetism describes the similarities between single domain particles and single magnetic ions. Both have spin(s) oriented in one direction that is field-dependent. However, unlike the effective moment associated with the isolated paramagnetic ion, the moment of a single domain particle is the sum of the

individual magnetic moments of ions comprising the solid, on the order of 10^5 contributing atoms. The magnetization curve of an assembly of superparamagnetic particles is single- valued (Mr=Hc=0) or lacks hysteresis. Magnetization occurs by particle rotation induced by an external magnetic field. At ambient temperatures, the effects of thermal agitation are sufficient to disorder the nanocrystalline particles in the absence of an external field. Thermal effects can be repressed if the system is cooled. As the temperature is lowered, the energy barrier between the lowest energy spin states of the particle is reduced and net magnetization increases. [11] Below a specific temperature, called the blocking temperature (T_b), superparamagnetism is destroyed and ferromagnetic behavior is observed (Figure 4). Also, magnetization curves of superparamagnetic material recorded at different temperatures above T_b superimpose when plotted as a function of Happ/ T (Fig.4). [12]

In addition to size and temperature, other factors which influence the magnetic properties of materials include: particle shape, distributions of particle size , isomorphic replacement, crystal lattice defects or dislocations, oxide core and surface composition [13], and particle-particle interactions. [14]

Figure 4. Magnetization curves illustrating the temperature dependence of superparamagnetic particles

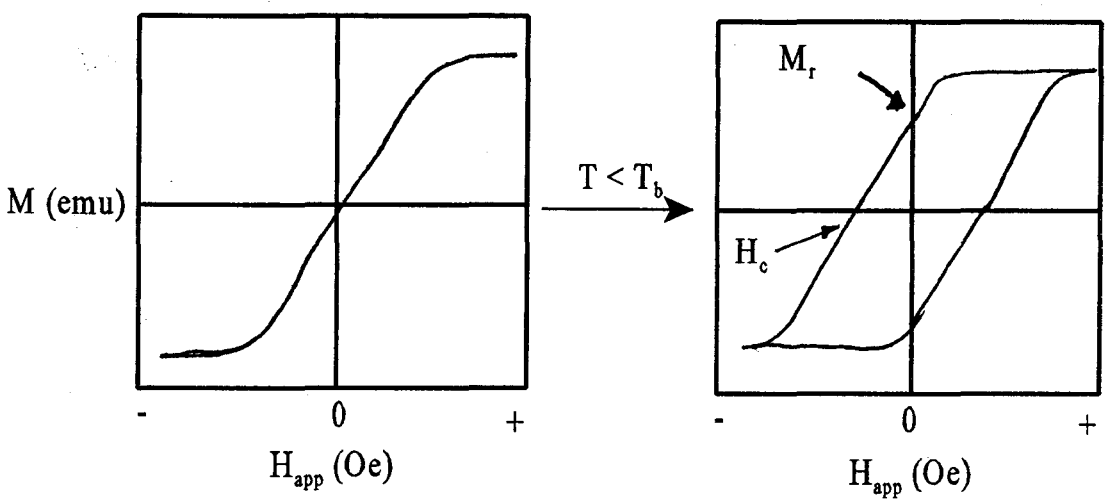

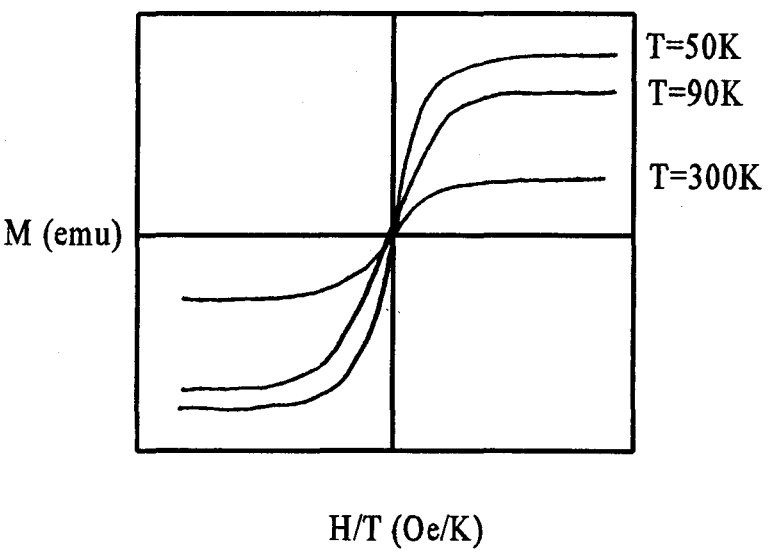

1.3. Preparation of Iron Oxides from Aqueous Fe^{2+}

The hydroxide, oxyhydroxide and oxide products resulting from the treatment of aqueous Fe^{2+} with alkali in bulk solution [15] are summarized in Figure 5.

1.4. Synthesis of Nanocrystalline Iron Oxide

The encapsulation of small magnetic oxide particles can be accomplished by high energy-high temperature methods, such as vapor deposition and aerosol spray pyrolysis, or by conventional 'wet chemistry' methodologies. Beside the obvious difference in scale and efficiency, the latter approach offers distinct advantages, namely control and fine tuning of the resulting composite properties. Both the submicron size of the magnetic oxide and the chemical nature of the encapsulating material impart unique properties to the product composite.

Most of the reaction pathways leading to the encapsulation of nanocrystalline magnetic particles can be categorized into two distinct, almost mirror-image, synthetic routes. One method begins with the co-precipitation of aqueous Fe^{2+} and Fe^{3+} by a strong base to form ultrasmall (d~10-20nm) particles of magnetite (Fe_3O_4) and maghemite (γ-Fe_2O_3).[16] The precipitated oxide particles have surface hydroxyl (OH) groups which can be modified by the addition of acid or base to form either OH_2^+ or OH^-. The magnetic sol can then be suspended by peptization, complexed electrostatically with a variety of charged surfactants, or coated with an inert material, such as silica, for stability and/or dispersion of the oxide in a solvent. [17]

Figure 5. Reaction pathways showing the possible oxide and oxyhydroxide products from aqueous Fe^{2+} treated with base, oxidizing agents and heat.[15]

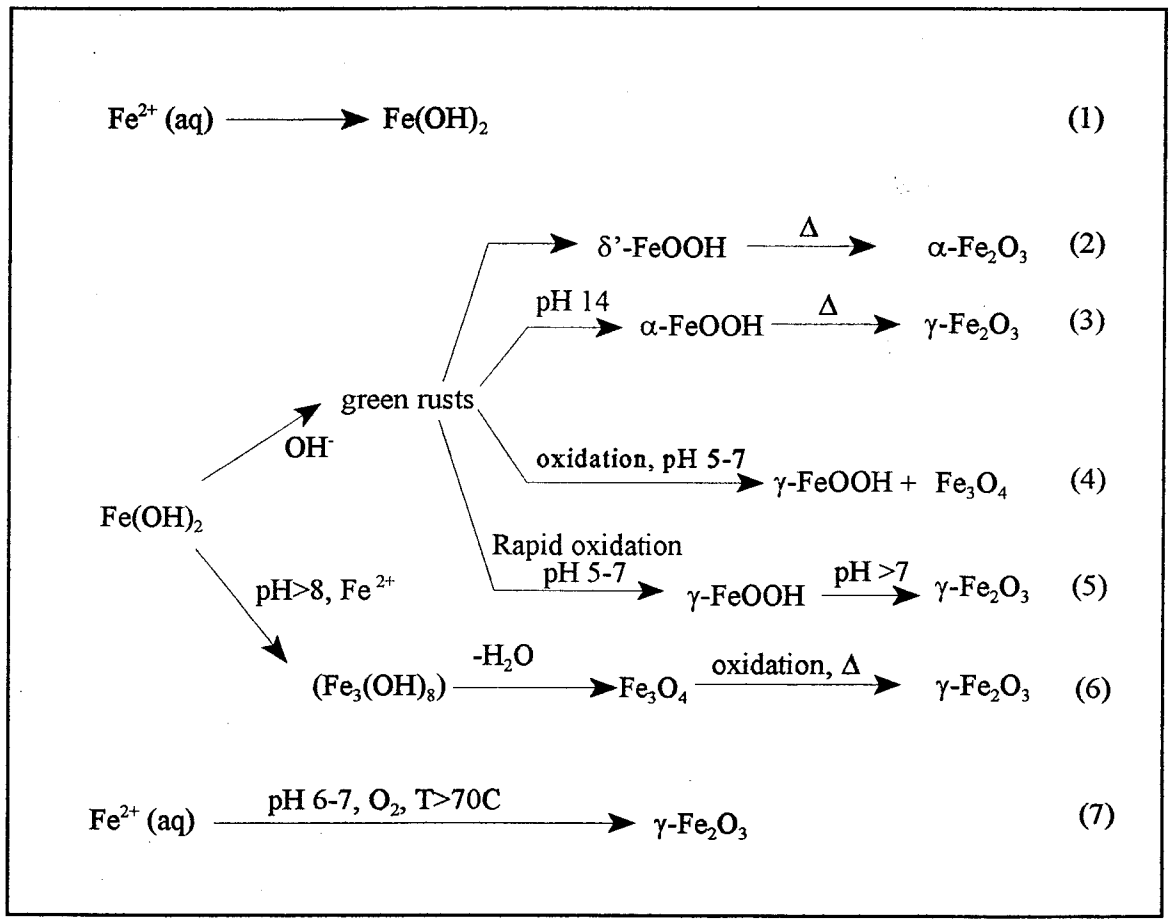

δ'-FeOOH	**Feroxyhyte**
γ-FeOOH	**Lepidocrocite**
α-FeOOH	**Geothite**
γ-Fe_2O_3	**Maghemite**
α-Fe_2O_3	**Hematite**
Fe_3O_4	**Magnetite**

In the second method, a pre-formed matrix or microenvironment acts as a template *into* which iron oxide is precipitated. The oxide is formed by either entrapment or binding of iron (II,III) cations followed by base hydrolysis then oxidation with an oxidizing agent such as hydrogen peroxide or oxygen gas. The matrix can be discrete (reverse micelles, lipids) or continuous (membranes, exchange resins, microspheres), neutral or ionic. The product typically has a distribution of isolated, ultrasmall oxide particles dispersed throughout the matrix or microstructure.

One unique aspect of the 'matrix- mediated' formation of iron oxide nanocrystals is the ability to 'recycle' the ionic matrix material through the reaction sequence, resulting in an increase in the size or concentration of the magnetic oxide. The concept of recycling the template was formulated by Ziolo at Xerox Corporation using cation exchange resins [18] and has been successfully applied to other ionic templates. In general, acidic resin protons are exchanged with divalent iron cations. Reacting the iron containing resin with a strong base results in the precipitation of an iron hydroxide intermediate. Oxidation of the iron hydroxide leads to the formation of an oxide particle. During the course of the reaction, the ion exchange sites are liberated and able to complex an additional equivalent of iron cations. The resin is then effectively recycled through the reaction process, iron exchange, base hydrolysis and oxidation, resulting in the growth and concentration of the oxide particles in the matrix and, consequently, the magnetism of the product composite. The 'loading capacity' of the matrix is dependent on both the physical constraints environment, such as degree of crosslinking, and the volume of active

reaction sites.

Both methods, direct formation of a magnetic sol by co-precipitation or *in situ* precipitation of iron oxide from complexed iron, have been used in the preparation of solid, liquid and gel phase iron oxide nanocomposites. The differences between the two methodologies are obvious: the direct method involves two steps, formation of the iron oxide followed by encapsulation, whereas the matrix method may involve numerous steps depending on the desired loading. The option to recycle the ionic matrix allows for control of magnetic properties unlike co- precipitation. However, co-precipitation typically results in the formation of submicron, spherical particles of magnetite and maghemite with a narrow particle size distribution. The same control over the iron oxide phase and particle morphology using the matrix method is not always observed. Both magnetic and non-magnetic, spherical and acicular shaped nanocrystalline iron oxides have resulted using the same reagents and reaction conditions on different matrix materials.

Beside the two general approaches described above, other methods exist for small particle synthesis. For example, nanocrystalline particles of iron oxide can be formed by the collision of two reverse-micelles: one micelle contains the aqueous iron salt and the other a strong base. [19] Indirect enzyme-catalyzed oxidation of entrapped iron cations has been performed using horse radish peroxidase [20] and jack bean urease [21]. Overall, the selection of one method over another is more or less tailored to the nature of the encapsulating material as well as to the intended application of the magnetic nanocomposite.

A common denominator between the seemingly different methodological paths is the presence of a barrier or protective layer surrounding the magnetic particle. Electrostatic, van der Waals, and/or steric repulsion effectively prevent flocculation of stabilized magnetic particles. Flocculation of small oxide particles results in the subsequent loss of unique magnetic, electrical, optical, and physicochemical properties associated with nanocrystalline iron oxides.

1.5. Biomimetics and Magnetic Biomaterials

Ultrafine magnetic iron oxide particles are found in both inorganic and organic species including rocks, minerals, magnetotactic bacteria, stingrays, chiton teeth, in the hair shaft of honeybees [22], and, as proposed recently, in surface layers of the human brain [23]. The goal of biomimetic investigations is to understand Nature's self-assembled, long-range and highly ordered submicron systems and to elucidate such efficient mechanisms for chemical synthesis. This is particularly relevant to the preparation of magnetic materials for in vivo applications where low toxicity and biocompatibility is a priority. Nanocrystalline iron oxides have been precipitated into both naturally occurring and synthetic or modified biomaterials. Examples of such systems and the properties of the constituent oxide are summarized in Table 1. The difference in particle phase and morphology between the various biological microstructures demonstrates the dependence of composite properties on the matrix or microenvironment.

Table 1. Examples of Organic Biomaterials as Templates for the Preparation of Small Particle Iron Oxides

Encapsulating Material	**Particle Morphology**			**Ref.**
	Iron Oxide	Particle Size (nm)	Shape	
Ferritin	$5Fe_2O_3$-$9H_2O$ Fe_3O_4	6 6	spherical spherical	24
Phospholipid Vesicles	FeO(OH), $5Fe_2O_3$-$9H_2O$, Fe_3O_4, Fe_2O_3	1.5-12	spherical, disc shaped	25
Carboxyalkyl ether polysaccharides	Various oxides and metal ferrites	3-30	na	26
Cellulosics	Fe_3O_4 γ-Fe_2O_3	5-10 10-70 (length)	spherical acicular	27
Dextran	Fe_3O_4	10-20	spherical	28
Gelatin	Fe_3O_4	5	spherical	29

1.6. Applications of Magnetic Biomaterials

Encapsulated magnetic materials have gained widespread use in medical diagnostics, imaging and drug delivery. Biocompatible encapsulating materials include starch, glycogen, polyamides, polyanhydrides and albumin. The two primary requirements of *in vitro* magnetic diagnostic agents include stability in the chemical environment of biological systems and low toxicity. The functional groups of the polymer stabilizing the magnetic particle can be modified to enhance the specificity of the composite to biological compounds. This technology has developed into magnetically-assisted separation techniques, examples of which include the selective separation of enzymes, cells, proteins, and DNA. Antigens and antibodies have also been affixed to magnetic substrates for immunological assays and detection of antiviral activity. [30]

1.7. Alginate

Alginate is a collective term used to describe polysaccharides occurring in the inner and outer cortex of various species of brown algae (Phaeophyta) and , to a lesser extent, in soil bacteria. In its native state, alginate exists as salts of alkaline earth cations present in the salt- water environment of the plant, including Mg^{2+}, Na^{+}, Ca^{2+}, Sr^{2+} and K^{+}. The polymer comprises 14-40%of the dry weight of algae and provides structural support of the algae fronds and acts as a salt water dessicator. Commercial alginate is extracted from dry seaweed and purified by dissolution of impurities using mild acid, base and methanol. The product is then precipitated with salts, hydrolyzed, and reconstituted

as sodium alginate with sodium carbonate. [31] Alginate is non-toxic. In foods and industrial products (Appendix I), alginate is used as an absorbant, emulsifier and stabilizer.

1.7.1. Structure of Alginate

The carbohydrate constituents of alginate, β-D-mannuronic acid (M) and its C5 epimer α-L-guluronic acid (G) are linked by (1→4) glycosidic bonds. Both residues exist in closed ring conformations with mannuronic acid in the $^4C_1$ conformation and guluronic acid in the $^1C_4$ conformation. The alginate backbone consists of blocks of each sugar residue (GGG, MMM) and of blocks of alternating or random sequences (MGMG, MMGMG) of varying length and frequency, as shown in Figure 6, depending on the source of the alginate. Circular dichroism [32] and ^{1}H and ^{13}C NMR [33] spectroscopy have been used extensively to identify the monomeric sequence and relative concentration of G and M residues in alginate samples. Both analytical methods rely on the physical properties associated with the different epimer conformations: NMR detects the different protons signals arising from monad (G, M), diad (GG, MM,GM, MG) and triad (MMG,GGM,GMG,MGM. etc) sequences, while circular dichroism is sensitive to the D- and L- conformations (not sequence) of the individual sugar units relative to standard polyM and polyG. The slight structural difference between the epimers, their relative concentration and their sequence have a strong impact on the chemical properties of the alginate in solution and gel phases. For instance, M blocks and G blocks are crystalline and resistant to acid hydrolysis while the regions of alternating sequences are amorphous

Figure 6. Conformation and sequence of sugar residues (M, G) in sodium alginate: (I) Alternating sequence of M and G, (II) G block sequence, and (III) M block sequence.

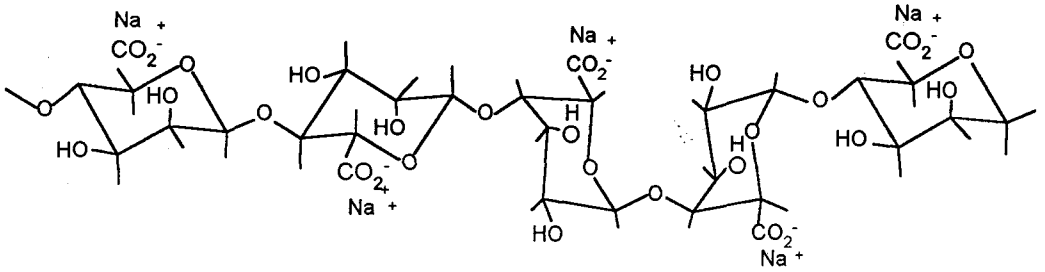

I

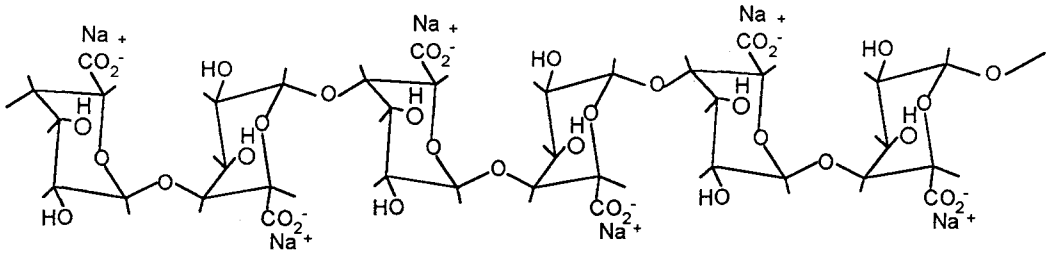

II

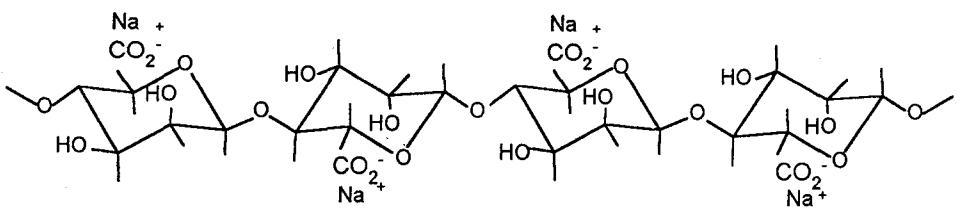

III

and easily hydrolyzed. [34]

The acid form of alginate, in which the C5 carboxyl groups are protonated, is water insoluble unlike the highly soluble sodium, potassium and monovalent salt derivatives. The polysaccharide is polydisperse with variations in molecular weight, degree of polymerization, and in concentration and sequence of the two sugars. The polymer adopts a random coil configuration in dilute solution. [32] Since alginate is a polyelectrolyte, its behavior in solution is strongly dependent on solution concentration, ionic strength, temperature and pH. This is reflected by the viscosity of aqueous alginate solutions.[35] Generally, viscosity decreases with increasing ionic strength, temperature, and pH but increases with concentration.

1.7.2. Gelation of Alginate

Alginate forms a dense three dimensional network in the presence of high concentrations of di- and tri-valent cations. Dilute solutions of alginate also bind cations but without macroscopic gelation. The mechanism, kinetics, cation selectivity, physical and rheological properties of alginate gelation have been studied extensively. Results from NMR, CD and ion exchange experiments suggest preferential and cooperative binding of cations to G blocks along the polymer backbone. Binding occurs to a lesser extent at MG sites but M blocks show little to no binding ability. [36] The preferential binding of cations by G blocks has foundations in the structural 1C conformation of G dimers. First, dynamic light scattering studies [37] and molecular modelling [38] have shown that the

extension of the different block compositions, which is governed by energies of rotation about the glycosidic bond, is greater for the M blocks than G blocks. In other words, rotation is more restricted for the poly G blocks for steric reasons. Second, the restricted 1C conformation of 1→4 linked G dimers results in an oxygen-lined pocket or cavity. The cavity is hydrophilic with a high charge density. The distance between carboxyl groups of adjacent G residues is 4.7-5.7 Å. Intrapolymeric binding of a di- or trivalent cation to G dimers is proposed to occur by pentadentate complexation involving the hydroxyl O3 and O2 of one G residue, the glycosidic O1, and the carboxylate O6 and pyranose ring oxygen of the adjacent unit.[39] The same is not observed with dimers of mannuronic acid. Crosslinking between G blocks of two polymer chains by di- and tri-valent cations is not as well understood as intrachain binding, but is proposed to involve both carboxylate and hydroxyl groups from G residues of different chains in close proximity. [40] The proposed structures of intra- and interchain cation complexed alginate are shown in Figure 7.

Ion exchange studies have shown that the affinity of cations to G blocks follows the sequence : $Pb^{2+} > Cu^{2+} > Cd^{2+} > Ba^{2+} > Sr^{2+} > Ca^{2+} > Co^{2+} = Ni^{2+} = Zn^{2+} > Mn^{2+}$. The binding affinites of Fe^{2+} and Fe^{3+} are not reported. [41] Physical properties of alginate gels, such as gel strength, optical transparency, pore size, stability and solute diffusion rates are a function of the concentration of G blocks. [42] Investigators report the most stable gels are those which contain a concentration of G>70% and which have an average G block length of 15 units or greater. Gels with a high G block concentration have

Figure 7. Binding of cations by alginate: Intrachain binding of cation to guluronic acid dimer (top) and interchain crosslinking to G block (bottom).

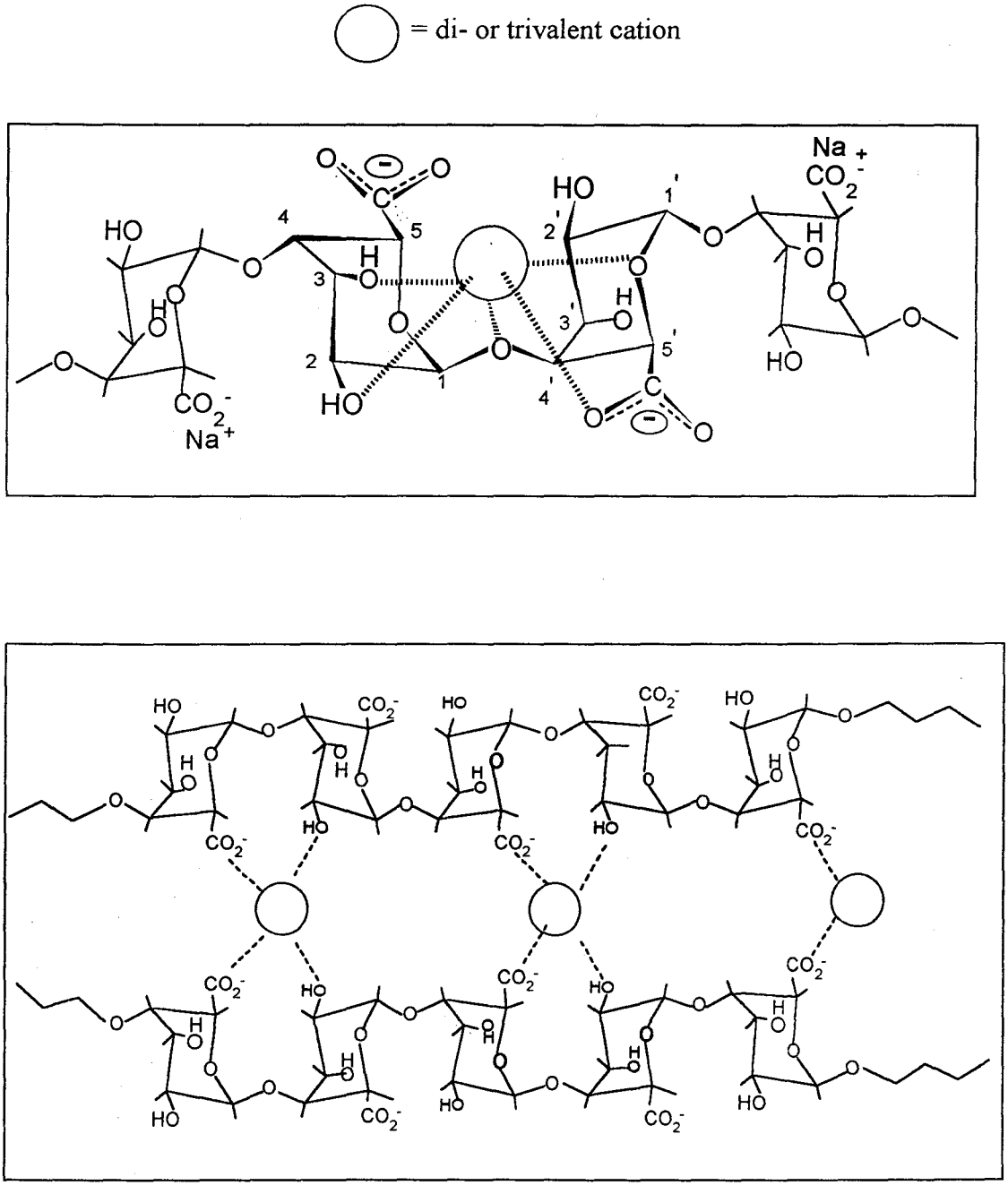

enhanced mechanical strength. The occurrence and length of mannuronic-acid sequences between the crosslinked junctions is proposed to play a role in the stability of the gel and pore size of the network.[42]

The phase transformation of aqueous alginate into a three dimensional network is also reversible. Cation sequestering agents such as EDTA , sodium citrate [43], phosphate buffers [41], and polyphosphates [31] are capable of liquifying the gels. Also, ion exchange of crosslinking cations by ions with a greater specificity for alginate can interrupt gelation.

1.7.3. Oxidative-Reduction Depolymerization

Carbohydrates are oxidized by free radical-generating reagents, oxidants such as H_2O_2, O_2, nitric and chromic acids, phenylhydrazine and permanganate, and enzymes and microbial species.[44] Free-radical oxidation reactions involve the transfer of electrons from the substrate to the oxidant. The reaction is initiated by irradiation or free-radical reagents. Homolytic cleavage of pyranose ring C-H bonds occurs with greater frequency at carbon centers adjacent to electron rich functional groups and/or the ring oxygen atom. The inductive effects of such groups stabilize the resulting substrate radical after departure of the hydrogen atom. Alcohol groups located at C5 are oxidized to ketones. The radical reaction mechanism that occurs with substrates having a C5 carboxyl substituent is illustrated in Figure 8.

Free-radical oxidation of hyaluronic acid, a linear glycosaminogylcan, and alginic acid,

Figure 8. Free-radical initiated beta-elimination at C5 of pyranose ring results in cleavage of the glycosidic bond. Hydroxy substituents at C2 and C3 were deleted for clarity.

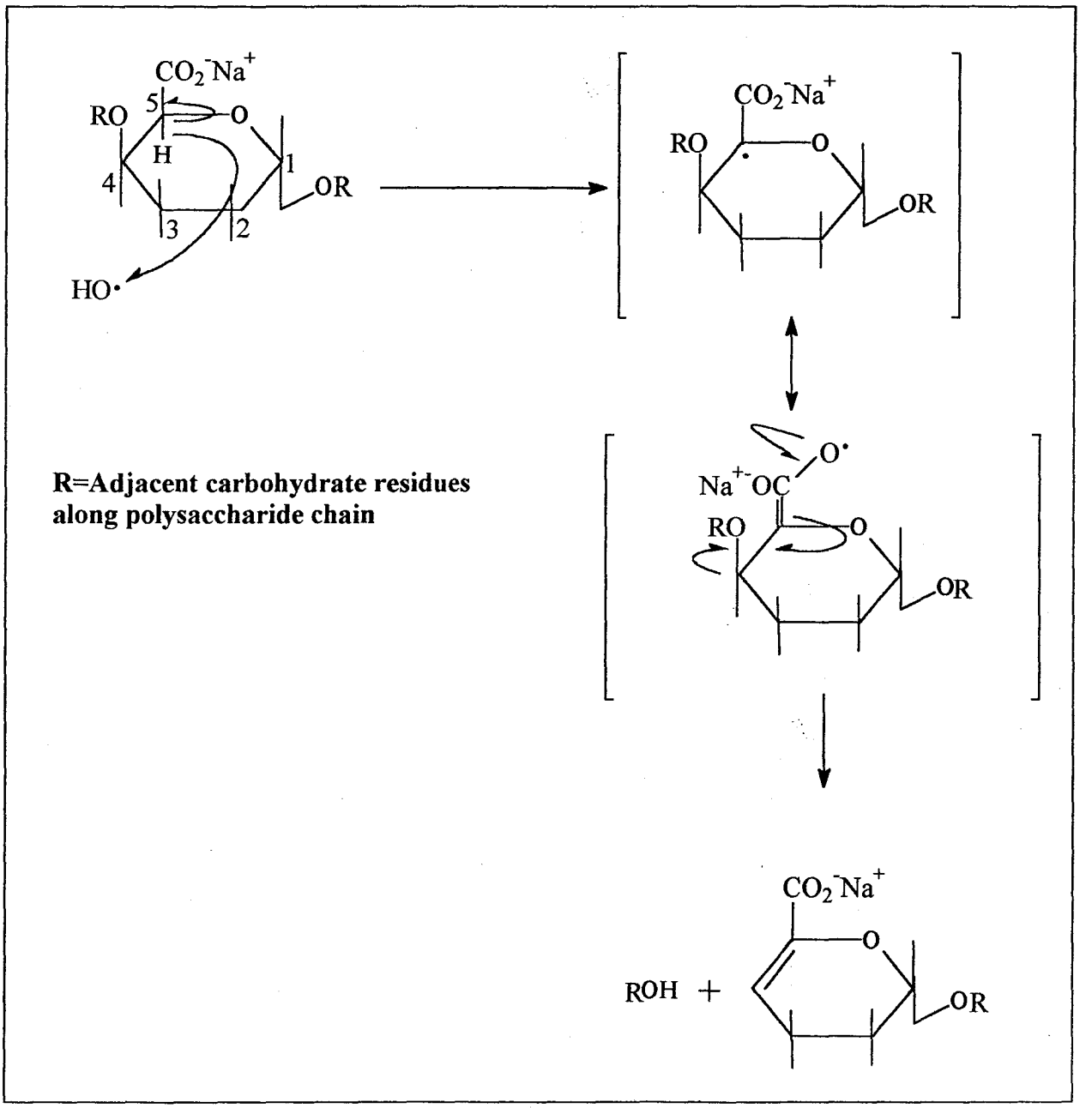

which have a carboxyl groups at C5 of the pyranose ring, is proposed to proceed by the mechanism in Figure 8. ESR experiments on irradiated hyaluronic acid have shown the occurrence of a radical intermediate.[45] β- elimination results in the cleavage of the glycosidic bond with concomittant irreversible polymer degradation. This results in a viscosity decrease, and a concurrent increase in the concentration of reducing end groups and 4,5-unsaturated uronic acid derivatives.[46] Both hyaluronic acid and alginic acid solutions exhibit similar behavior with respect to the depolymerization effects of autoxidants.

Active free radicals are a prerequisite for polysaccharide degradation. Hydrogen peroxide and oxygen (O_2) are two common free-radical precursors. However, the activity of the peroxide, monitored by the rate of substrate degradation, is significantly enhanced when the peroxide is combined with organic reducing agents and metal ions. Reducing agents are defined as compounds or metal ions which readily donate electrons. Organic reducing agents are numerous [47] and include quinones, thiols, and enediols. The compounds possess a labile hydrogen which is capable of activating or reducing molecular oxygen and peroxide. Metal ions, including iron (II,III), copper (I,II), cobalt (II,III) and tin (I,II), which readily interconvert between stable oxidation states are also potent reducing agents. Activated molecular oxygen initiates the generation of hydroperoxy radicals. Hydrogen abstraction by this radical intermediate generates an active substrate radical. Cleavage of C-H occurs preferentially at carbon centers with carboxyl group substitutents as opposed to alcohol groups. The oxidation reaction proceeds with chain

propagating and terminating steps involving the reducing agent, the peroxide and the substrate.

Hydrogen peroxide dissociates into hydroxyl radicals. The activity of H_2O_2 is reduced in acidic, neutral and polar solvents. The effectiveness of the peroxide and the susceptibility of the polysaccharide toward oxidation are enhanced under alkaline conditions and in the presence of metal ions. Metal ions act in an analogous fashion to organic reducing agents but are more potent even in micromolar concentrations. Fentons' reagent, composed of ferrous salt and hydrogen peroxide, generates hydroxy radicals which oxidize secondary alcohols to ketones.[44] The cyclic oxidation/reduction of Fe^{2+} and Fe^{3+} is perpetuated in the presence of organic reducing agents, such as ascorbic acid, and molecular oxygen or hydrogen peroxide.

Degradation is negligible for solutions of aqueous alginic acid and ascorbic acid under anaerobic conditions.[48] However, the viscosity of alginate ($10gL^{-1}$), after three hours of exposure to 0.01M ascorbic acid at 20°C and open atmosphere, is reduced from 3000cP to 9cP. The rate of alginate degradation at pH 6 with 0.01M ascorbic acid is approximately 150 times faster than in the presence of 0.01M hydroquinone. The difference in reactivity of the reducing agents is related to the equilibrium of radical-forming and radical -destroying reactions. The equilibrium is dynamic and dependent on both the concentration of the reducing agent and its relative ability to become oxidized. Radical-destroying mechanisms are proposed to dominate in polysaccharide solutions with high reducing agent concentrations (>0.1M) which would

explain the observed inhibitory effects.[49]

Depolymerization is inhibited under anaerobic condition, by radical destroying enzymes (catalase) and radical scavengers such as ($Fe(CN)_6^{4-}$) and alcohols.[50] Inhibitory effects are also observed in solutions containing high concentrations of halides (F<Cl<Br<I) and organic solvents, such as acetates and alcohol. The repression of degradation in solutions containing methanol, ethanol, propanols and butanols has been reported yet not fully explained mechanistically. However, the rate of polysaccharide degradation decreases with increasing concentration and molecular weight of organic alcohol solvents.[51] The independent effects of pH, temperature, and radiation must also be considered when examining the origins of polysaccharide degradation. For instance, naturally-occurring phenolic impurities in commercial grade alginic acid are known to cause depolymerization.[52]

2. PREPARATION OF FE $^{2+}$-CROSSLINKED AND IRON OXIDE ALGINATE HYDROGEL BEADS AND MAGNETIC FLUID

2.1. Materials

The following chemical reagents were used in the preparation of magnetic alginate hydrogels and liquids:

Alginic Acid, Sodium salt	Aldrich	Lot #03326EG
Ferrous chloride hexahydrate	Fischer	
Sodium hydroxide	BDH	
Reagent Grade Methanol	Caledon	
Sodium phosphate	BDH	
NANOpure Deionized Water		

2.2. Synthesis of Iron(II)-crosslinked Alginate Hydrogels

Iron crosslinked-alginate hydrogels were prepared at room temperature by dropwise addition of aqueous sodium alginate ($30gL^{-1}$) from a 25 mL buret, equipped with a 17 gauge stainless steel syringe needle, into a degassed solution of ferrous chloride dissolved in 1:1 (v/v) methanol : water. In a typical preparation, 250mL of 0.1 M $FeCl_2$ (25mmoles) solution was degassed with N_2 in a 500mL roundbottom flask sealed from the atmosphere with rubber septa. The needle of the buret was then inserted normal to the iron salt solution at a height of approximately 15 cm above the surface of the liquid. The average rate of addition of aqueous alginate to the ferrous chloride solution was 55 drops per minute.

Spheres or beads, *ca.* 2mm in diameter formed instantaneously. The gel beads were allowed to remain in solution for twenty-four hours under static nitrogen atmosphere. The beads were washed with copious amounts of 1:1 (v/v) methanol:water to remove excess iron. Excess iron in the washes was detected by Quantafix Fe^{2+} indicator paper or by spot-test reaction with 0.5 M NaOH in a test tube. The crosslinked beads were opaque and pale yellow in color.

2.3. Formation of Iron Oxide within the Hydrogel Matrix

Iron oxide formation was initiated by addition of 200mL of aqueous sodium hydroxide (0.5M, pH 14) to methanol:water saturated (~50mL) Fe^{2+}- crosslinked beads while under inert atmosphere in the roundbottom flask. Exposure of the iron crosslinked gel beads to base resulted in an immediate color change from pale yellow to dark green. The beads remain dark green colored for the two hour duration of alkaline treatment.

Oxidation of the microspheres was performed by bubbling oxygen into the solution. Within 30 minutes of oxygenation, the beads changed color from green to pale orange. The beads were washed a second time with 1:1 (v/v) methanol: deionized water to neutral pH. The above procedure resulted in the formation of 'first-loaded' hydrogels.

This procedure was repeated an additional four to five times using iron-oxide containing beads. For instance, first-loaded beads were exposed to calculated volumes of degassed 0.1M $FeCl_2$ (1:1 v/v methanol: water) in a round bottom flask, under inert atmosphere, were rinsed, reacted with base for two hours followed by oxygenation for

two hours. The result were second loaded hydrogels. The volume of reagents used were scaled according to the initial volume of sodium alginate, ie 25mL alginate ($30gL^{-1}$): 250mL $FeCl_2$ (0.1M): 200mL NaOH (0.5M). This procedure was repeated up to six times with Fe^{2+} crosslinked alginate hydrogels.

Water-saturated Fe^{2+} - crosslinked and iron oxide-alginate beads are stable and can be stored indefinitely in 1:1 methanol:water without evidence of disintegration or leaching of iron from the gels. Gel beads were dehydrated using a vacuum freeze dryer.

2.4. Preparation of Magnetic Liquid from Magnetic Hydrogels

Sixth loaded gel beads were removed from the water/methanol by decantation. They were then subjected to sonication for one hour at 25°C, which resulted in the destruction of gel structure. Aqueous sodium phosphate (pH 7.03, 1.0 mM, 15mL) was added to the resulting disintegrated beads and sonication was repeated. High molecular weight material was removed by centrifugation (9500 rpm, 8 minutes). After centrifugation, the liquid was decanted and transferred to a clean centrifuge tube and centrifugation (9500rpm, 8 minutes) was repeated. Pressure filtration (N_2, 20psi) was then performed using an Amicon 850 ultrafiltration cell equipped with a 30,000 MWCO glycerol-coated filter membrane and magnetic stirrer. Concentration proceeded until 70% of the initial volume was removed as filtrate. The final solution was recovered from the filtration unit with a pipette and stored in a glass vial.

A schematic diagram showing the overall preparation of Fe^{2+} -crosslinked and iron-oxide containing alginate gel beads and the magnetic liquid is shown in Figure 9.

Figure 9. Preparation of magnetic alginate hydrogel beads and iron oxide- alginate colloids from Fe^{2+}-crosslinked alginate.

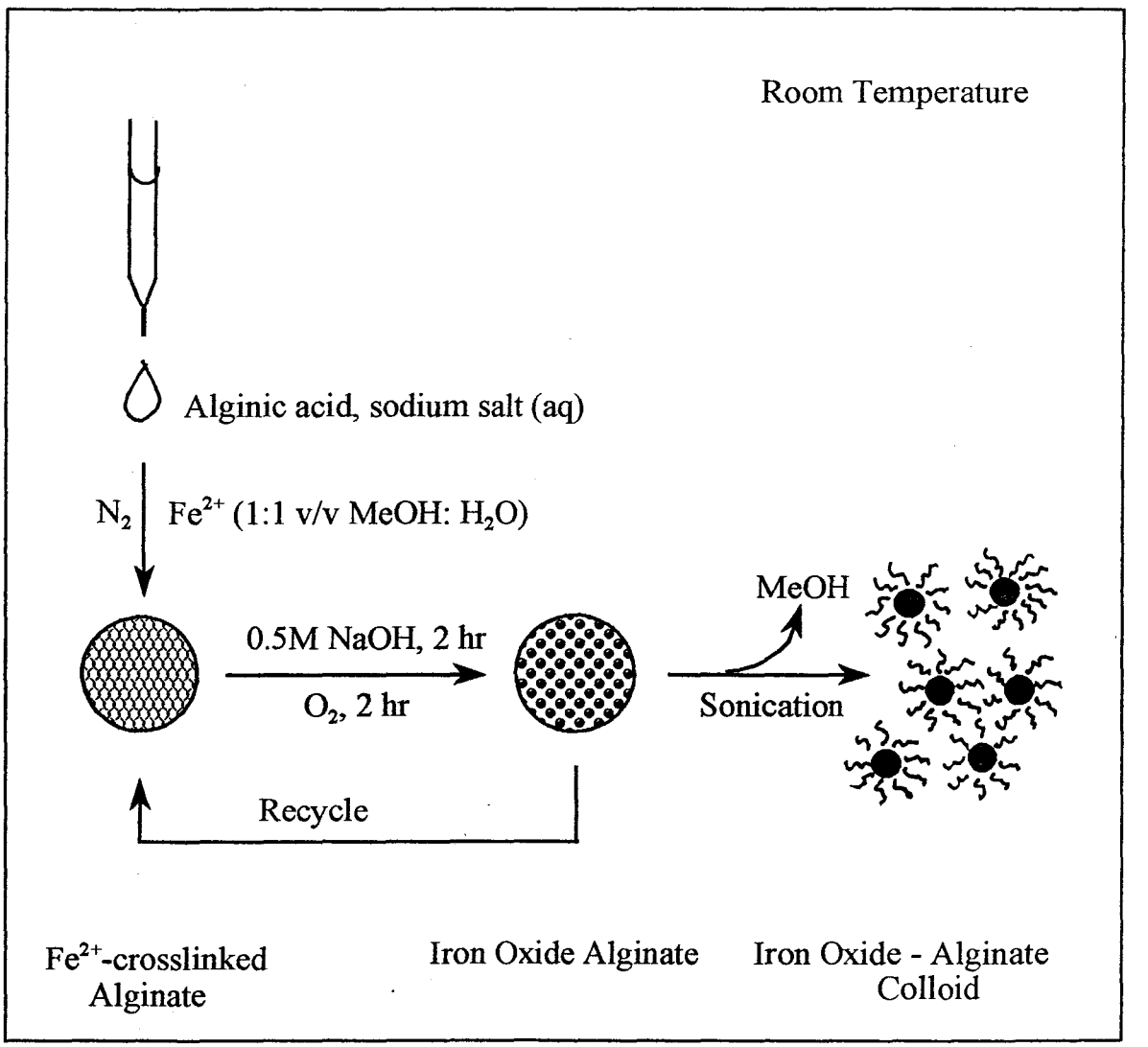

3. CHARACTERIZATION TECHNIQUES OF FE $^{2+}$-CROSSLINKED AND IRON OXIDE ALGINATE HYDROGEL BEADS AND MAGNETIC FLUID

3.1. Molecular Weight of Sodium Alginate

The average molecular weight of linear polymers can be estimated by performing viscosity measurements using the relationship between intrinsic viscosity ([η]) and molecular weight (Eq1). The values of K and a depend on the nature of the polymer and on the solvent.

$$[\eta]=KM^{a} \qquad (1)$$

K and a have been estimated from log-log plots of different alginates with varying molecular weight and intrinsic viscosities. In NaCl solution (0.1M), K is reported as $2.0x10^{-5}$ dL/g and a assumes a value of unity under theta conditions. [53]

Four concentrations (0.25, 0.50, 1.00, 1.25 g/dL) of sodium alginate were prepared by dissolving the polymer in 0.1M NaCl overnight. Aliquots (8mL) were introduced into a dry Cannon-Fenske Viscometer (#200) and allowed to equilibrate to 25°C. Constant temperature was maintained using a temperature controlled circulating water bath. The kinematic viscosity (centistokes) of each solution was calculated from averaged efflux times and the viscometer constant (K= 0.10335 at 25°C). The viscosity of aqueous sodium chloride was 1.02cP. The reduced viscosity (dL/g) of each alginate

solution was calculated and plotted as a function of solution concentration (g/dL) as shown in Figure 10.

3.2. Concentration of Carboxylate Groups [54]

A solution of sodium alginate (5.55 gL^{-1}, 90 mL) was prepared with 0.001M NaCl as the solvent. Aqueous sodium hydroxide (0.1M, 5 mL) was added to the solution prior to titration. The titration was performed with constant stirring using 0.2 - 0.5 mL of 0.1M HCl. The conductivity (cell constant K=1.05cm) of the solution was monitored and recorded for each addition of acid (50mL total). The solid content of the solution following titration was determined by evaporation of the solvent and weighing the dry product. The specific conductance of alginate as a function of the volume of HCl is shown in Figure 11.

3.3. ^{1}H NMR Determination of M Block:G Block Concentration in Sodium Alginate

^{1}H NMR was used to estimate the relative concentration and sequence of mannuronic and guluronic acids in sodium alginate. The M and G sugar residues of sodium alginate exist in homogenous, alternating and random block sequences along the backbone of the polymer. Regions of alternating and random sequences are easily hydrolyzed while the homogenous block sequences are more resistant to hydrolysis. The fixed structural conformation of M and G and the limited number of interactions by adjacent sugar residues give rise to characteristic proton signals. [55] Anomeric proton

Figure 10. Intrinsic viscosity of sodium alginate.

Concentration of Sodium Alginate (g/dL)	η_{sp} /conc.
0.25	4.35 ± 0.02
0.50	5.90 ± 0.02
1.00	10.76 ± 0.03
1.25	14.53 ± 0.09

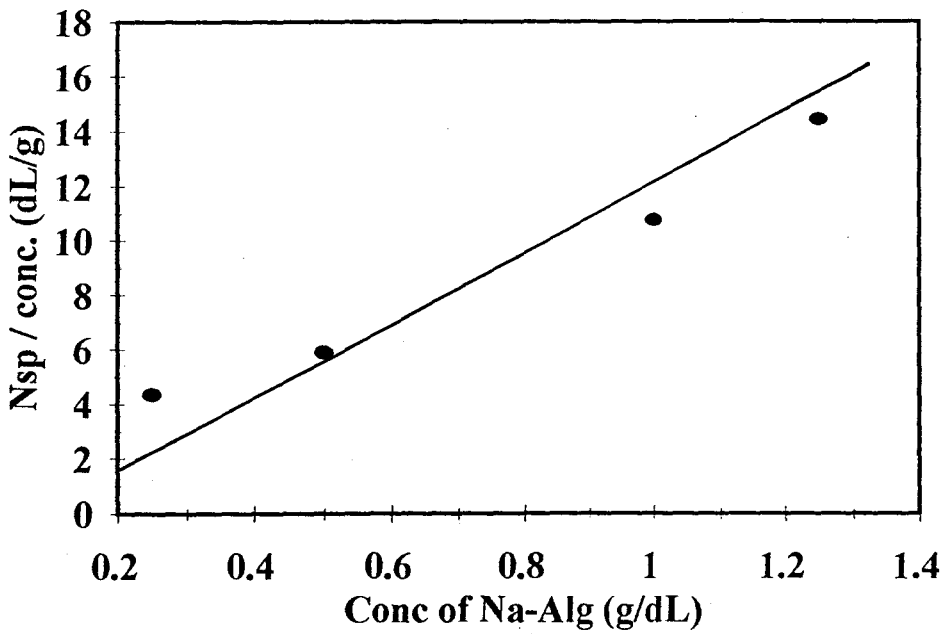

Figure 11. Conductometric titration of sodium alginate CO_2^- groups.

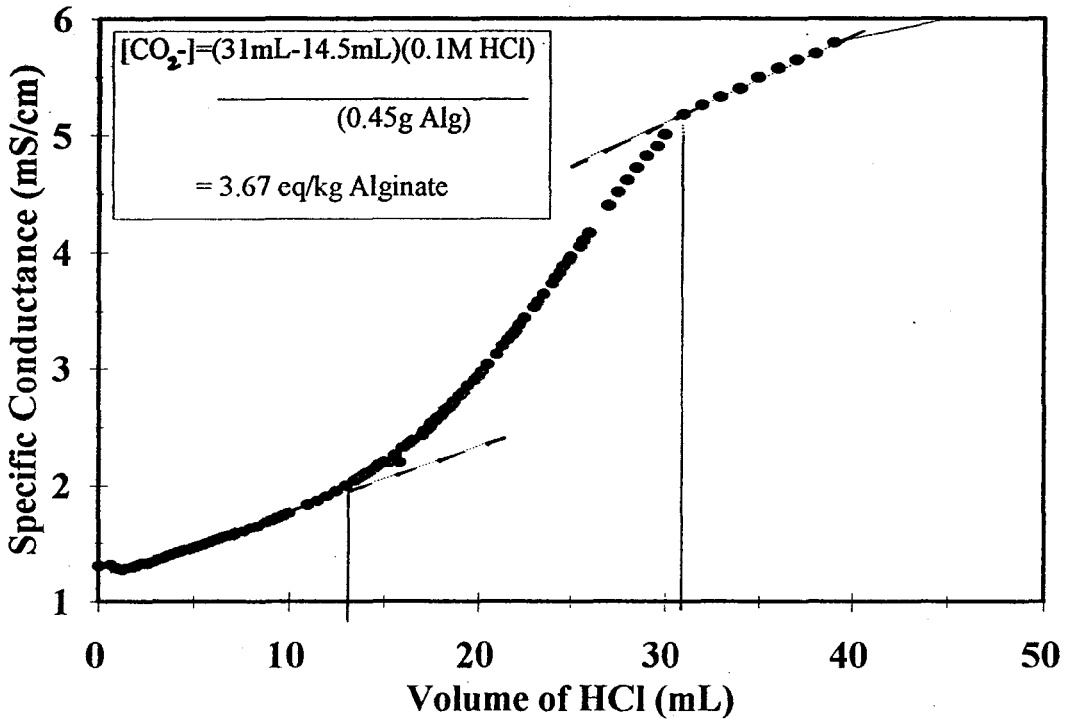

signals from M (H-1) and G(H-1, H-5) and from MG, used to estimate the molar ratio of G and M sugar residues in alginate, occur between 5.5 - 4.0 ppm. Proton signal assignments for diad and triad sequences of M and G can also be made from a proton NMR spectrum. [56]

Whole and hydrolyzed sodium alginate were characterized by ^{1}H NMR. Residual impurities were removed from sodium alginate by allowing the solid to stir for 24hr in 1:1 methanol: water. The product was filtered and freeze-dried. Whole alginate is then subjected to acid hydrolysis in order to remove regions of alternating sequences, which result in proton signal overlap. Following a literature procedure [56], hydrolyzed samples were prepared by acidifying aqueous sodium alginate (10.0 g L^{-1}) with 0.1 M HCl, added in 0.5 mL aliquots, until pH 3. The solution was then heated to T=98-100°C for thirty minutes,cooled then centrifuged (9500 rpm,10 min). Centrifugation resulted in the collection of a slurry which was separated from the milky supernatant by decanting. The slurry was resuspended in 10 mL of water and centrifuged once more (9500 rpm,10 min). The product was freeze-dried and stored under N_2.

Samples for NMR analysis were weighed (~4mg) and dissolved in deuterated water (~1.5mL) in thin-walled glass NMR tubes. 3-(Trimethylsilyl) -tetradeutero sodium propionate (3mg) was used as an internal reference (0.0 ppm) in all alginate samples. The ^{1}H NMR spectra were recorded at 90°C using a Bruker AC 300 NMR Spectrometer with the assistance of Brian Sayer. Inversion recovery programming (5.3 sec pulse delay) was

used during the analysis of hydrolyzed alginate to partly eliminate and shift the HDO signal away from the low-field anomeric proton region.

3.4. Gel Permeation Chromatography (GPC) of Sodium Alginate Solutions

GPC analysis was performed to determine the stability of alginate solutions using a Waters 510 gel phase chromatography system. Aqueous alginate ($30gL^{-1}$) solutions ranging in age from 2 days to six months were analyzed by gel phase chromatography. The Waters ultrahydrogel column (7.8mm I.D., 30 cm length) was calibrated with polyethylene oxide ($1gL^{-1}$) standards of known molecular weight. The Waters instrument operating manual recommended 0.1M aqueous sodium nitrate as the solvent for the separation and analysis of polysaccharides. One polyethylene oxide standard (570,000 Daltons) was dissolved in 0.1M $NaNO_3$ ($1gL^{-1}$) and injected to compare the retention time with that of aqueous PEO. All alginate solutions were prepared by diluting 1mL of aqueous solution with 9 mL of filtered and degassed 0.1M $NaNO_3$. The volume of injected alginate sample was 100 μL and the flow rate was set at 0.7mL/min. Both UV (Waters 486, λ=215 nm, 260 nm) and refractive index (Waters 410, T_{int} = 30°C) detectors were used to analyze the eluants of the column.

3.5. Iron Quantification of Iron(II)-crosslinked and Iron Oxide Alginate Hydrogels and Magnetic Fluid

The quantitative analysis of iron (Fe^{2+}) in crosslinked and iron oxide containing alginate gel beads was performed by standard colorimetric procedures using

1,10-phenanthroline.[57] The sample preparation and analytical procedure are described in detail in Appendix II. In general, iron forms a six-coordinate complex with phenanthroline ($[Fe(phen)_3]^{2+}$) giving rise to a highly colored solution. The iron concentration of the initial solution is calculated from the measured absorbance of the solution at λ=510 nm and the experimental absorption coefficient. All measurements were done in triplicate.

3.6. Gravimetric and Volume Analysis of Swollen Hydrogel Beads

The percent solid of Fe^{2+}- crosslinked and iron oxide containing alginate gels was determined by gravimetric analysis. Nitrogen gas was used to remove the excess solvent from the surface of a bead before recording the hydrated mass. The beads were then dehydrated in an oven at 90°C for 2-3 hours then allowed to cool to room temperature. Percent solids per bead was calculated from the difference in weight of the dry and hydrated gels. Ten to fifteen gel beads from a given loading were measured in bulk then averaged in order to account for any discrepancies in bead volume or density.

The volume of swollen Fe^{2+}- crosslinked and iron oxide containing alginate beads was calculated using the equation of volume for a sphere ($4/3\ \pi\ r^3$). Gel beads were transferred, with solvent, to a glass Petri dish. The diameter of each bead was measured using a vernier caliper (0.02 mm). Five to ten measurements of different beads from the same batch were made then averaged.

3.7. FTIR Characterization of Sodium Alginate and Alginate Derivatives

Alginate samples for FTIR (Bio-Rad FTS-40) characterization were freeze-dried then mixed (~1:9) with solid potassium bromide. A die press (15,000 psi) was used to make a transparent pellet for analysis. A nitrogen atmosphere (10psi) was maintained during the recording of each spectrum.

3.8. Powder X-Ray Diffraction Analysis of Dehydrated Iron Oxide-Alginate Gels

Samples (10-50mg) submitted for powder X-Ray analysis were freeze-dried and ground to a fine powder using a mortar and pestel. The Nicolet I2 diffractometer was operated with CuKα (λ = 1.5401Å) x-ray source and scintillation detector. Diffraction data ($10 < 2\theta < 80$ degrees, 10-40 min.) was collected by Mr. Gong in the BIMR X-Ray Laboratory.

3.9. Thermal Gravimeteric Analysis (TGA) / Differential Scanning Calorimetry (DSC) of Sodium Alginate and Gels

Sodium alginate and dehydrated gels samples were submitted to Mr. H.F.Gibbs for TGA/DTA (Netzsch STA) analysis. Samples were heated (10°C/ min) from 25°C to 800°C using an aluminum oxide crucible and reference. Solid samples were heated in an air atmosphere (30 cc/ min) while beads were heated under nitrogen (10cc/min).

3.10. Magnetization Measurements using SQUID Magnetometer

Temperature and field dependent magnetization measurements of samples were performed using a Quantum Design MPMS SQUID Magnetometer. Samples for analysis

were freeze-dried and accurately weighed. Sample weights ranged from 5-20 mg. The solid was transferred to a water soluble gelatin capsule. The void volume of the capsule was filled with Kimwipe tissue to prevent sample movement during measurements. The capsule was then loaded into a drinking straw and manually inserted into the liquid helium cooled SQUID sample compartment. Measurement sequences were programmed and executed with the MPMS software. Magnetization curves at 30kOe and 5K, 25K, 35K, 50K and 300K were collected.

3.11. Transmission Electron Microscopy (TEM)

Water swollen beads were treated first with propylene oxide then embedded in a Spurr's epoxy resin which was fixed at 70°C. The solid specimen was microtomed and mounted for imaging. The accelerating potential of the JEOL JEM 1200 EXII TEMSCAN Microscope was 50 keV. Gel sample preparation and TEM analysis were performed by Mrs. Marcie West of the Electron Microscopy Lab located in Life Sciences (McMaster University).

Ferrofluid samples were deposited onto a carbon grid and exposed to a heat lamp for solvent evaporation. A thin film formed on the grid. The imaging quality of ferrofluid samples was improved when samples were filtered through a sterile 0.45 μm filter prior to evaporation. Bright field photomicrographs and selected area electron diffraction patterns of the composite were taken with the assistance of Fred Pearson in the BIMR Microscopy Lab using a Phillips CM12 Electron Microscope operating at 120 keV.

3.12. Dynamic Light Scattering of Magnetic Fluid

The colloid dimensions and solution properties of the ferrofluid were investigated using dynamic light scattering. Light scattering data were collected using a Brookhaven Instruments BI9000 AT instrument with an argon laser (λ=514.5 nm, 90° scattering angle) at 25°C. The refractive index detector was set at 2.9 Re. Concentrated ferrofluid (<10μl) was diluted with solvent in a 50mL volumetric flask. Solvents included water, aqueous NaCl (0.1M, 0.01M) and aqueous tetrabutylammonium chloride (0.01M). The pale-yellow colored liquid (20-25mL) was filtered through a fresh 0.45 μm filter into a clean light-scattering vial.

3.13. Capillary Electrophoresis (CE) of Magnetic Fluid

Capillary electrophoresis was used to determine the electrophoretic mobility, zeta potential and relative purity of the alginate ferrofluid at constant applied potential (25kV, 30kV) and temperature (23°C). The CE instrument (ATI Unicam Crystal CE Model 310, Water 991 Photodiode array detector (λ=254nm)) used had a capillary with a total length of 90cm, an effective length of 60cm, 50 mm I.D., and 100 mm O.D. Samples were prepared by diluting ferrofluid (50 μl) in sodium phosphate buffer (1mM) of varying pH (5.95, 7.02, 7.93, 9.03, 10.03, 11.06). The injection volume of sample was 6.14 μl. Caffeine was used an internal neutral marker.

4. RESULTS AND DISCUSSION

4.1. Properties of Sodium Alginate

Sodium alginates, of differing molecular weight ranges, are commercially available. The tan-colored granular solid purchased from Aldrich has a viscosity of 200-400 cP for $30gL^{-1}$ of aqueous sodium alginate. The salt form of alginate was soluble in water (pH 5-8) but insoluble in methanol and acidified aqueous solutions.

The molecular weight of the starting material was determined from viscosity studies of dilute sodium alginate solutions. The intrinsic viscosity of alginate was found to be 1.35 ± 0.05 dL/g which, when using the literature values of a and K for identical alginate solutions, corresponds to an average molecular weight of 67,525 ± 250 amu. The molecular weight of freshly prepared alginate analyzed by GPC, with a molecular weight calibrated column, was ~22,400 . Both techniques are not absolute methods of determining MW, however, the value obtained by viscosity studies was chosen to be more accurate. GPC results may have been more quantitative had the column been calibrated with polysaccharide standards as opposed to PEO.

Each sugar residue of sodium alginate possesses one carboxylate group. The $[CO_2^-]$ of aqueous sodium alginate, determined by conductometric titration, was ~ 3.67 eq kg^{-1} alginate. The concentration of carboxylate groups of sodium alginate was similar to

that of sodium *O*-(carboxymethyl) cellulose fibers ($[CO_2^-]$ ~3.42 eq kg^{-1}).[54]

As mentioned earlier, the relative concentration and sequence of sugar residues of alginate is source dependent. The product information sheet from Aldrich provides the M:G ratio (1.4: 1.95), but the source of sodium alginate was not quoted. The low-field ^1H NMR spectra of whole and hydrolyzed alginate are shown in Figures 12 and 13, highlighting the anomeric proton signals. The molar concentration of M and G and the M block: G block ratio was calculated from published equations relating the origin and intensities of anomeric proton signals for M (H-1), G(H-1, H-5) and MG(H-5).[58] Proton signal assignments and the calculated molar ratio of M and G sugar residues of whole and hydrolyzed sodium alginate are summarized in Table 2.

Table 2. Composition and Distribution of M and G Residues in Whole and Hydrolyzed Sodium Alginate.

Residue (proton)	Chemical Shift*	Composition	
		Whole	Hydrolyzed
M (H-1)	4.67	0.607	0.542
G (H-1)	5.05	0.393	0.457
(H-5)	4.46		
Diad Frequency			
MG (H-1)	4.70	0.201	0.061
MM (H-1)	4.67	0.406	0.481
GG (H-5)	5.05	0.192	0.396

* Chemical shifts in ppm downfield from internal tsp-*d4*.

Figure 12. 300 -MHz FT ^{1}H NMR spectrum of sodium alginate recorded in D_2O at 90°C.

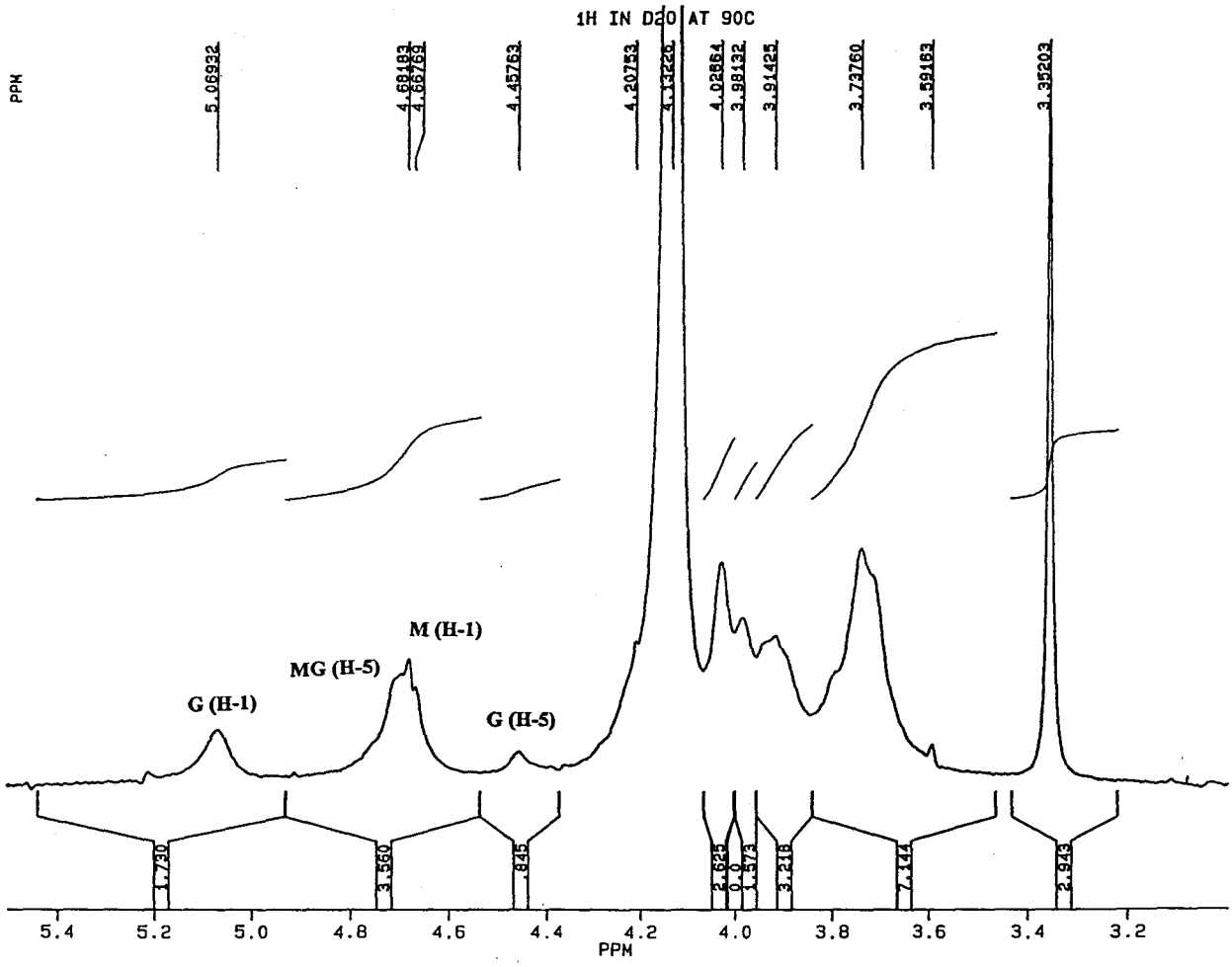

Figure 13. 300-MHz FT ^{1}H NMR spectrum of alginate fractionated by hydrolysis recorded in D_2O at 90°C.

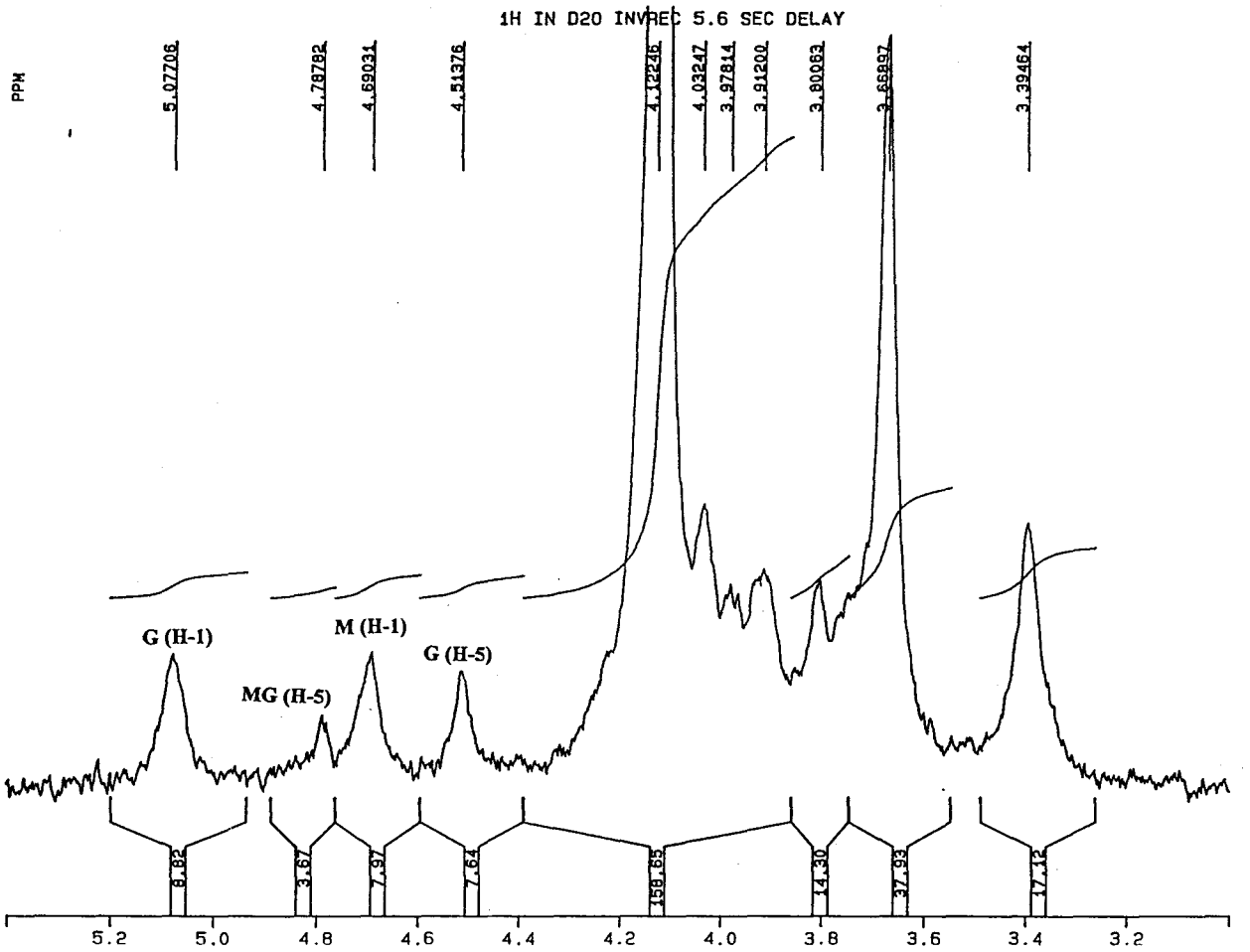

The M:G ratio of the sodium alginate used was found to be 0.61M : 0.39G. In the unhydrolyzed alginate sample, the low-field proton signal for MG(H-5) had the largest intensity signifying a high concentration of alternating and/or random sequences of M and G. After hydrolysis, the intensity of this signal decreases, as expected. The M block:G block ratio, calculated from the respective anomeric proton signal intensities in the spectrum of the hydrolyzed sample, was found to be 0.48: 0.39. The appearance of the low-field proton signals of whole alginate and the calculated M:G block ratio of the hydrolyzed sample is identical to alginates isolated from the seaweed *Laminara digitata*. [58]

Phenolic compounds and enzymes are natural contaminants of alginic acid. Polyphenols, in low concentrations, are known to depolymerize alginate. Aqueous alginate solutions ($30gL^{-1}$) became discolored, decreased in viscosity and became more turbid with age. GPC traces of fresh (<2days) aqueous alginate revealed a predominant band (97%) centered at 18.6 minutes. As the age of the solution increased (2days<t<6mo), the intensity of this band decreased and the concentration of lower molecular weight material increased (Figure 14). The presence of aromatic contaminants in solution was confirmed by absorption of UV at λ=260nm. Suggested purification methods of alginate include multiple washes with methanol and acetic acid. Alginate, used in the preparation of iron-crosslinked and iron oxide containing gels, was dissolved in water overnight and used within two days.

Figure 14. GPC elution profile of sodium alginate solutions: 2 days after preparation (top) and 5 months after preparation.

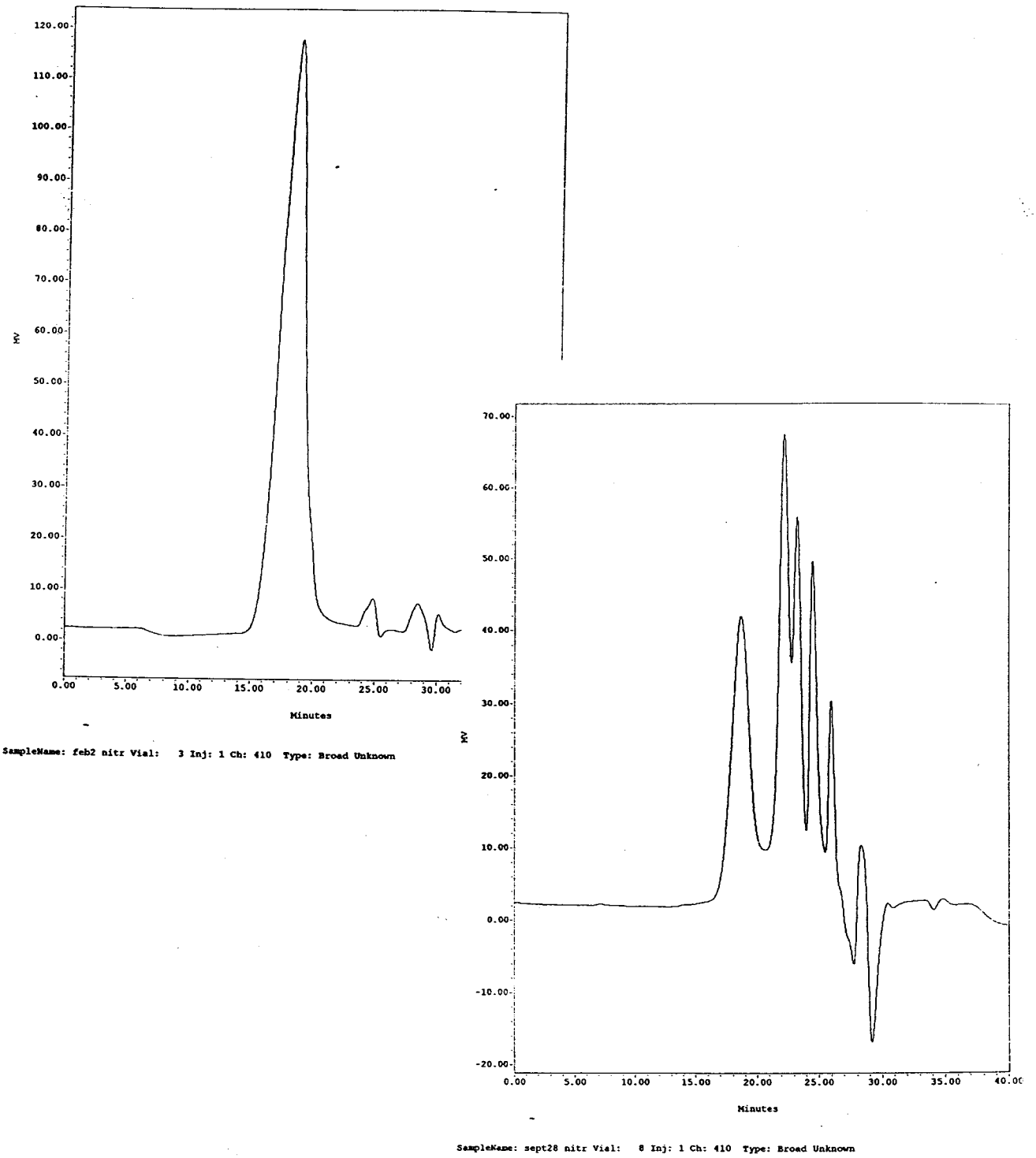

4.2. Iron-Crosslinked Alginate Beads

Three batches of iron crosslinked and iron-oxide containing alginate beads were prepared according to the procedure outlined in Sections 2.3-2.4. One batch was taken through five consecutive loadings while the remaining two were carried through six reaction cycles. Crosslinking of alginate ($30gL^{-1}$) in ferrous chloride solution results in the complexation of 2.3 ± 0.5 mmole of Fe per gram of alginate, as determined from iron quantification. This quantity is independent of the number of hours the beads were left in the ferrous chloride reaction solution (Figure 15). Also, the average quantity of Fe^{2+} complexed by alginate did not change when crosslinking was performed in the absence of methanol. The time-independent complexation and narrow standard deviation of iron concentration in crosslinked samples suggest a regularity in the binding of Fe^{2+} cations by alginate. Error may be due to insufficient rinsing of uncomplexed iron from the beads prior to elemental analysis.

The degree of crosslinking of alginate by iron cations can be estimated from the results of iron quantification and conductometric analysis. Assuming carboxylate groups complex Fe^{2+}, 2.3 mmole of Fe corresponds to 62% of total [$-CO_2^-$] participation of sodium alginate.

Figure 15. The concentration of iron complexed by alginate is independent of the amount of time the beads are exposed to excess Fe^{2+} in the reaction solution after crosslinking.

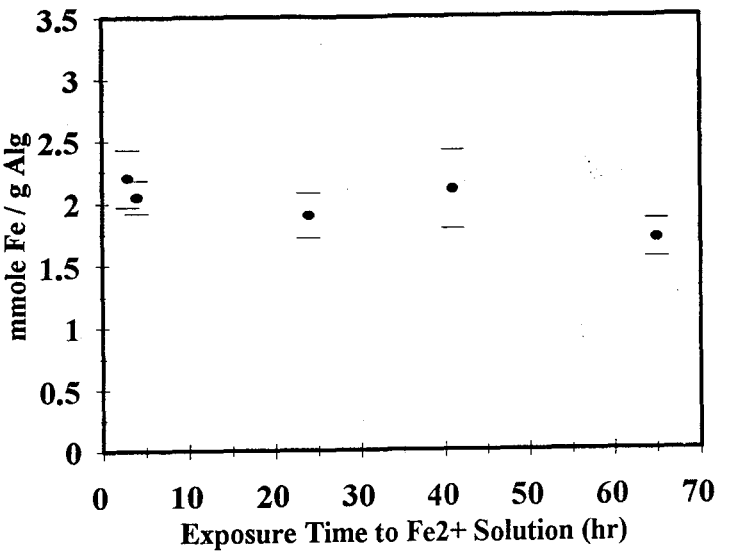

4.3. Iron Oxide-Alginate Beads

The formation of nanocrystalline iron oxide within alginate gels was reproducible. Three general trends are observed as the number of loadings of iron oxide into the gel matrix increases: (1) the total quantity of Fe was increased, (2) the magnetization increased, and (3) the diameter or volume of the swollen beads decreased. Total iron concentration as a function of loading, averaged from three batches, is shown in Figure 16. The amount of iron in first loaded beads was within standard deviation of the crosslinked precursors following base hydrolysis and oxidation. This result indicates that ferrous cations are bound strongly to the polysaccharide. Approximately 15.1 total

mmole, or 0.85 total g, of Fe were complexed, from crosslinked gel to six loadings, per gram of alginate. The adsorption of ferrous cations from solution, prior to base hydrolysis and oxidation, steadily increased from first to fourth loadings then appeared to 'saturate' with higher loadings.

Figure 16. Average concentration of iron from three batches of iron-crosslinked (Loading 0) and iron oxide alginate gel beads (Loadings 1-6).

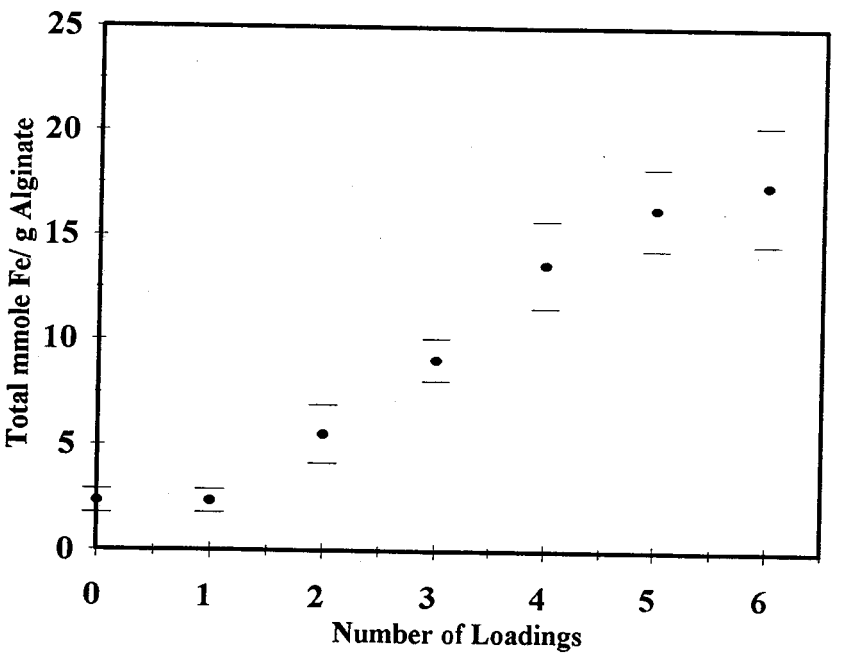

Iron crosslinked beads were pale yellow in color. The methanol:water saturated crosslinked beads became dark green within one minute after the addition of NaOH. The

observed color occurred both in the interior and at the surface of the bead. The green color was attributed to the formation of iron hydroxy salts or 'green rusts' typically observed as intermediate in the base catalyzed hydrolysis of Fe^{2+} to various oxyhydroxides and oxides (Fig. 5, Eq 2-7).

Green colored beads rinsed to pH 6 with methanol:water became orange within 24 hours. The change in color may be attributed to oxidation of iron hydroxide to iron oxide by water, air, and/or molecular oxygen. The rate of oxidation was increased by bubbling gaseous oxygen into the alkaline solution containing the beads, resulting in the same color change from green to orange but within one hour. Further change in color or intensity of color was not observed when beads were bubbled with oxygen for an additional hour. SQUID measurements of first loaded beads show superparamagnetic behavior, although not macroscopically observable. The orange color and magnetism suggest the presence of an ordered, ultrasmall iron oxide crystal.

A minimum of 10%(v/v) methanol was required to maintain the structural integrity of the iron crosslinked bead during base hydrolysis. Beads remained stable and became green colored in alkaline solutions without methanol but collapsed if agitated by shaking or bubbling nitrogen into the soultion. Methanol was used in all reactions and in the rinsing solutions to inhibit oxidative-reductive depolymerization of alginate. Degradation occurs in the presence of oxygen and iron cations; therefore, disintegration of the gel in the absence of methanol could result from oxidative-reductive depolymerization. Because alginate is insoluble in methanol, polymer precipitation may also stabilize

the gel. For instance, Fe^{2+} is the crosslinking agent which, upon addition of base, is hydrolyzed to green rust or iron hydroxide. If the gel crosslinks are broken with the formation of $Fe(OH)_2$, then poor solvent quality may inhibit the dissolution of alginate.

Ferrous ions were adsorbed from solution by beads that contain iron oxide. Two potential reaction sites are possible for the adsorption of iron: the polysaccharide and the oxide particle surface. In aqueous environments, metal oxide particles have charged surfaces at the solid-solution interface resulting in the electric double layer.[59] Iron cations may be adsorbed to the surface of the iron oxide particle within the polysaccharide network (Figure 17).

Figure 17. Schematic diagram showing the possible mechanisms of Fe^{2+} adsorption to the surface of iron oxide particles with active surface hydroxy groups.

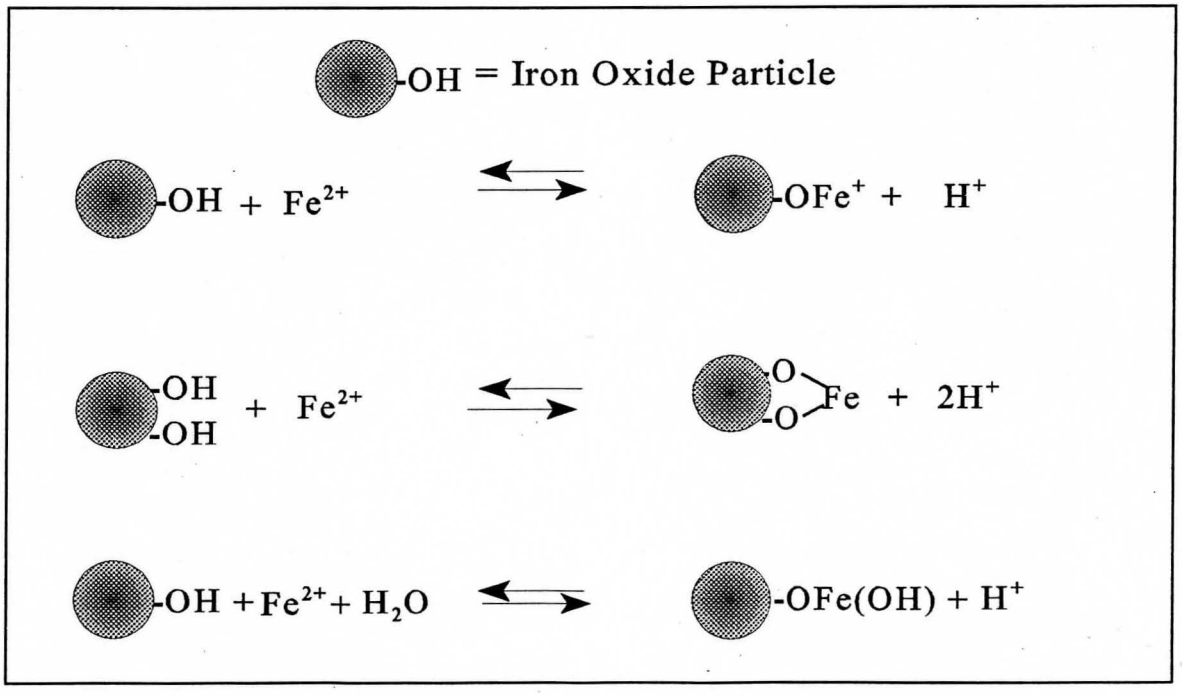

The concentration of adsorbed iron to an oxide particle is a function of the concentration of reactive sites on the particle surface, competition between Fe^{2+} and other cations (Na^+, H^+) in solution, and equilibrium reactions occurring at the interface. Reactive alginate sites, including carboxylate and hydroxide groups, if liberated during the previous hydrolysis/oxidation of iron, may complex a second equivalent of Fe^{2+}. Unlike the regulated adsorption of iron by alginate during crosslinking, the two sites of iron adsorption would explain the increased margin of standard deviation observed in the total concentration of Fe with loadings 2-6.

Gravimetric /Volume Analysis

The results of gravimetric and dimensional analysis of gels containing iron and iron oxide are summarized in Figure 18. The measured weight difference was attributed to a loss of water and/or an increase in solid content with the growth of iron oxide particulates. The alginate polymer and iron oxide comprise the solid content of the dehydrated gel beads. From first to six loadings, the Fe: alginate ratio increases from 0.11g Fe:g polymer to 0.86 g Fe: g polymer. As the percent weight of solid material increased with higher loadings, the bead volume decreased from 11.7 mm^3 to 4.3 mm^3. Volume reduction can be attributed to increased crosslinking occurring between chains with loading or to the neutralization of functional groups. However, both pH dependent swelling behavior and FTIR studies indicate that the alginate gel network remains ionic. For instance, the alginate polymer in water swollen gels becomes protonated in 0.1N HCl.

Protonation of the carboxylate groups causes the gel to shrink from ~2mm to 1mm. When swollen alginate gels are exposed to 0.1M NaOH, the diameter of the bead increases from ~2mm to ~4mm. With the exception of the first loading, volume reduction with loading reflects increased crosslink density and stronger chemical interactions occurring between the polymer and iron oxide particle. Structural changes in the polymer were examined using infrared spectroscopy.

Figure 18. Solid content and volume of swollen iron-crosslinked and iron oxide alginate beads.

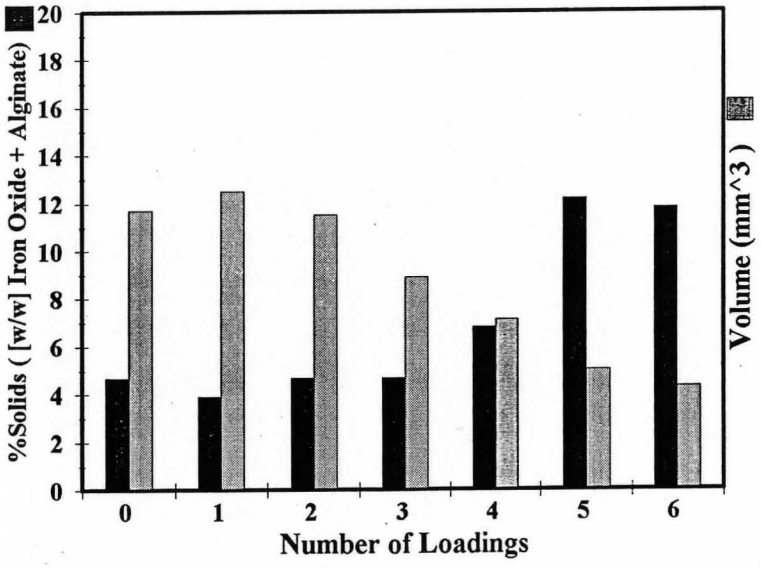

Fourier Transform Infrared Analysis of Alginate Composites

The FTIR spectrum of sodium alginate is shown in Figure 19. The strongest signals include the strong and broad band associated with the stretching (3430 cm^{-1}) and deformation (1200-1100cm^{-1}) of the polymeric hydroxyl group and two bands assigned to ionized carboxylate groups (1635-1540; 1430-1300 cm^{-1}). The position and intensity of the hydroxyl bands are diagnostic of the presence or absence of intermolecular bonding and hydrogen bonding.[60]

When alginate is crosslinked by Fe (II,III) cations in the presence of methanol: water, the -OH stretching band becomes broad and is shifted to slightly lower wavenumbers, 3398 cm^{-1} for Fe^{2+} (Figure 20) and 3417 cm^{-1} for Fe^{3+}, indicating a weakening of the O-H bond. The polysaccharide remains ionic as demonstrated by the presence of the strong, ionized carboxylate signals at 1616 cm^{-1} and 1419 cm^{-1}. The appearance of a weak band at 1735 cm^{-1}, the carboxylic acid (CO_2H) stretching frequency for alginic acid, indicates that a small portion of alginate became protonated during crosslinking.

Earlier investigations of the reactivity of alginates, prior to the full elucidation of alginate as a heteroglycan, reported the methylation of alginate carboxylate groups at room temperature and under rather mild conditions by exposure to acidic methanol.[61] Esterification or quenching of the reactive ionic sites of alginate would result in two changes: alginate would become insoluble and complexation of cations to alginate would be prevented. In order to investigate whether methylation of alginate occurred under the

Figure 19. FTIR spectrum of sodium alginate.

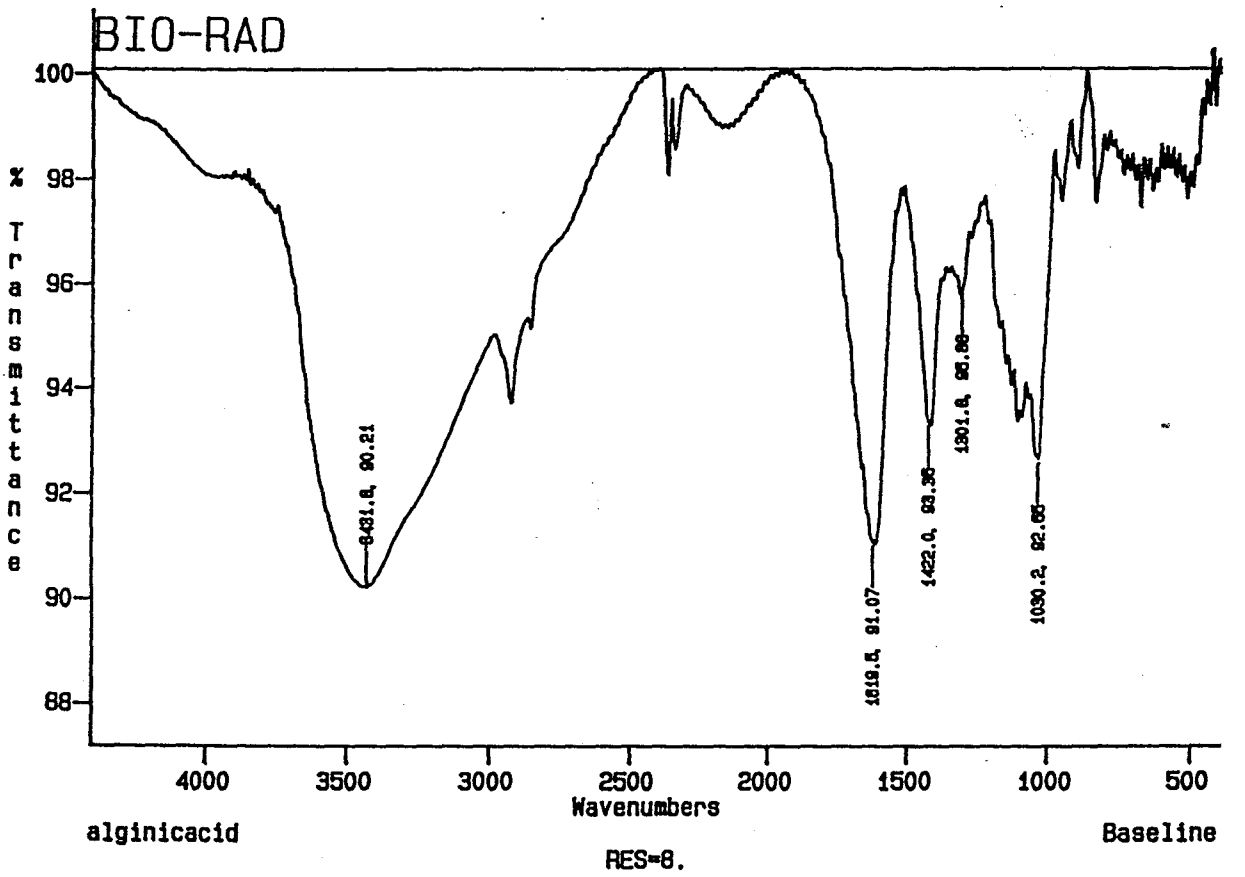

Figure 20. FTIR spectrum of Fe^{2+}- crosslinked alginate.

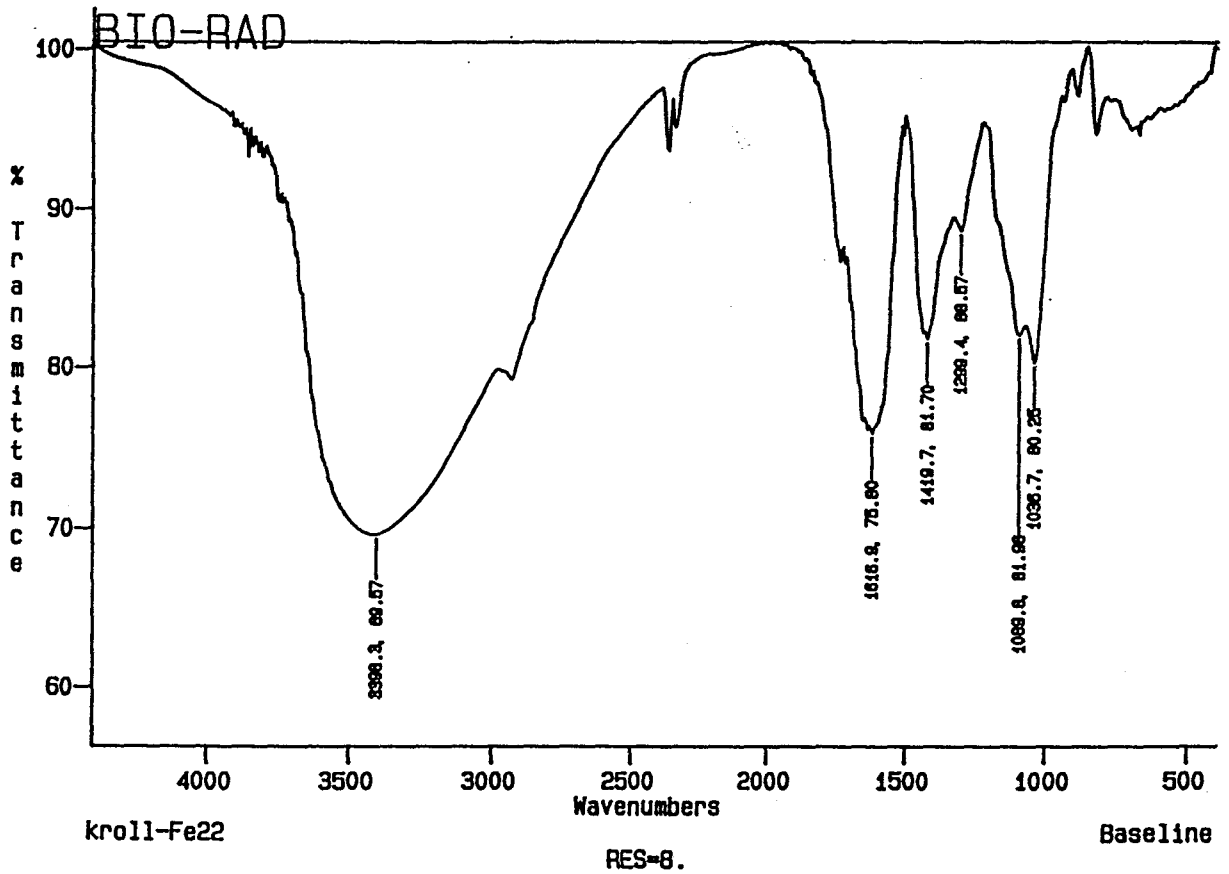

present reaction conditions, samples of sodium alginate were reacted with pure methanol, aqueous HCl (0.1M, pH1), and 1:1 v/v methanol: 0.1M HCl, isolated and characterized with FTIR. The spectrum of alginate exposed to methanol was identical to that of aqueous sodium alginate. The spectrum of alginate exposed to acid exhibited a new strong CO_2H band at 1735 cm^{-1}, a new band of medium intensity at ~1250cm^{-1} , and the second carboxylate band at ~1420 cm^{-1} decreased in relative intensity (Figure 21). Additionally, the -OH band at 3422 cm^{-1} became narrower and strong at 1200-1000 cm^{-1}. The absence or weak intensity of the CO_2H (1735 cm^{-1}) and CO_2CH_3 (1250 cm^{-1}) signals in the spectra of crosslinked alginate suggest little to no occurrence of esterification or protonation of alginate under the reaction conditions used in the preparation of magnetic beads.

Two significant changes occurred in the FTIR spectrum of alginate after six reaction cycles (Figure 22). First, the -OH band shifted approximately one hundred w-avenumbers from ~3440 cm^{-1} to 3300 cm^{-1} and decreased in intensity. The shift of the hydroxyl group indicates a weakening of the alginate -OH groups, signifying interaction with the iron oxide particle. The stretching vibrations of the carboxylate group also shift to lower wavenumber with the asymmetric stretch of OC=O and C-O- shifting from 1617 to 1601cm^{-1} and 1418 to 1406 cm^{-1} , respectively. Second, a strong band appeared at ~604 cm^{-1} which was absent in the spectrum of crosslinked alginates. The occurrence of this band coincides with the formation of iron oxide. Its frequency is in the range (700-400cm^{-1}) associated with Fe-O stretching and O-Fe-O deformations of maghemite and

Figure 21. FTIR spectrum of hydrolyzed alginate. The FTIR spectrum of alginate reacted with pure methanol (not shown) is identical to the spectrum of sodium alginate (Fig 19).

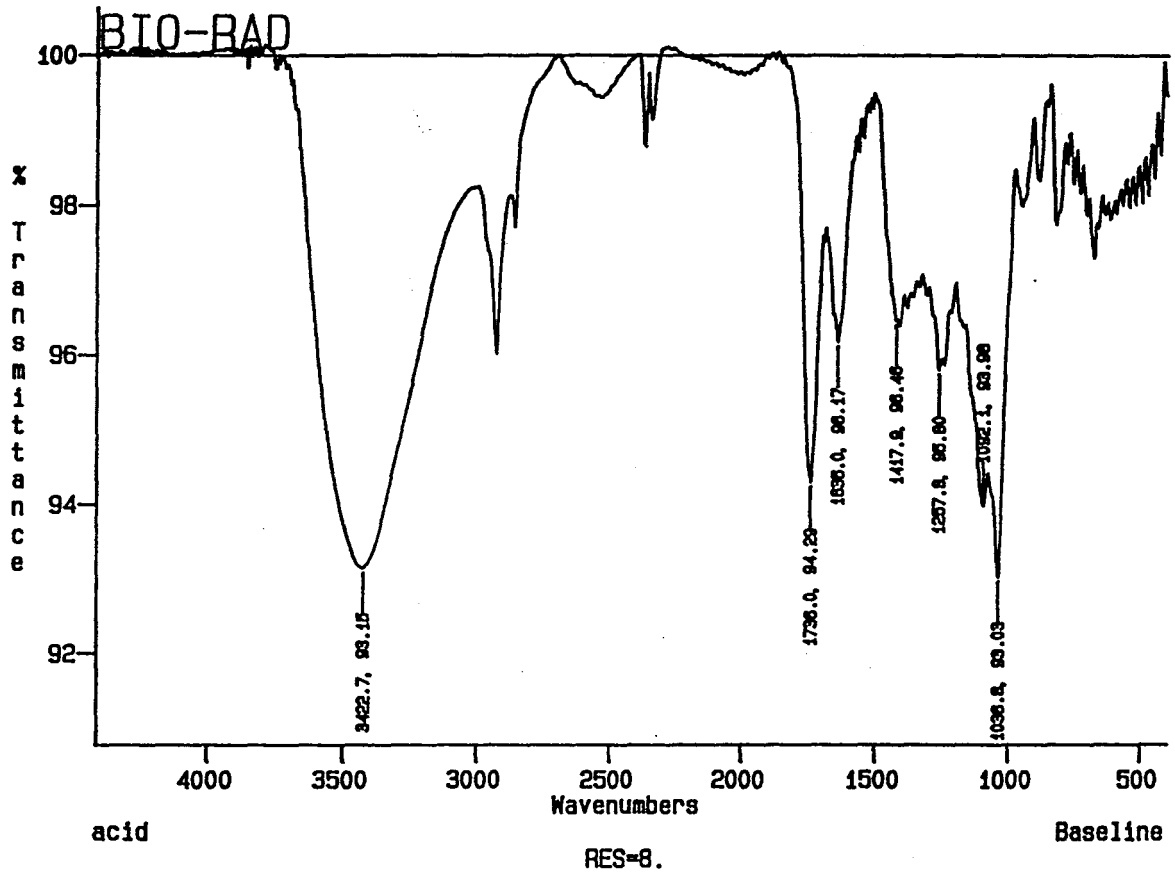

Figure 22. FTIR spectrum of Fe^{2+}-crosslinked alginate taken through six reaction cycles of base hydrolysis and oxidation.

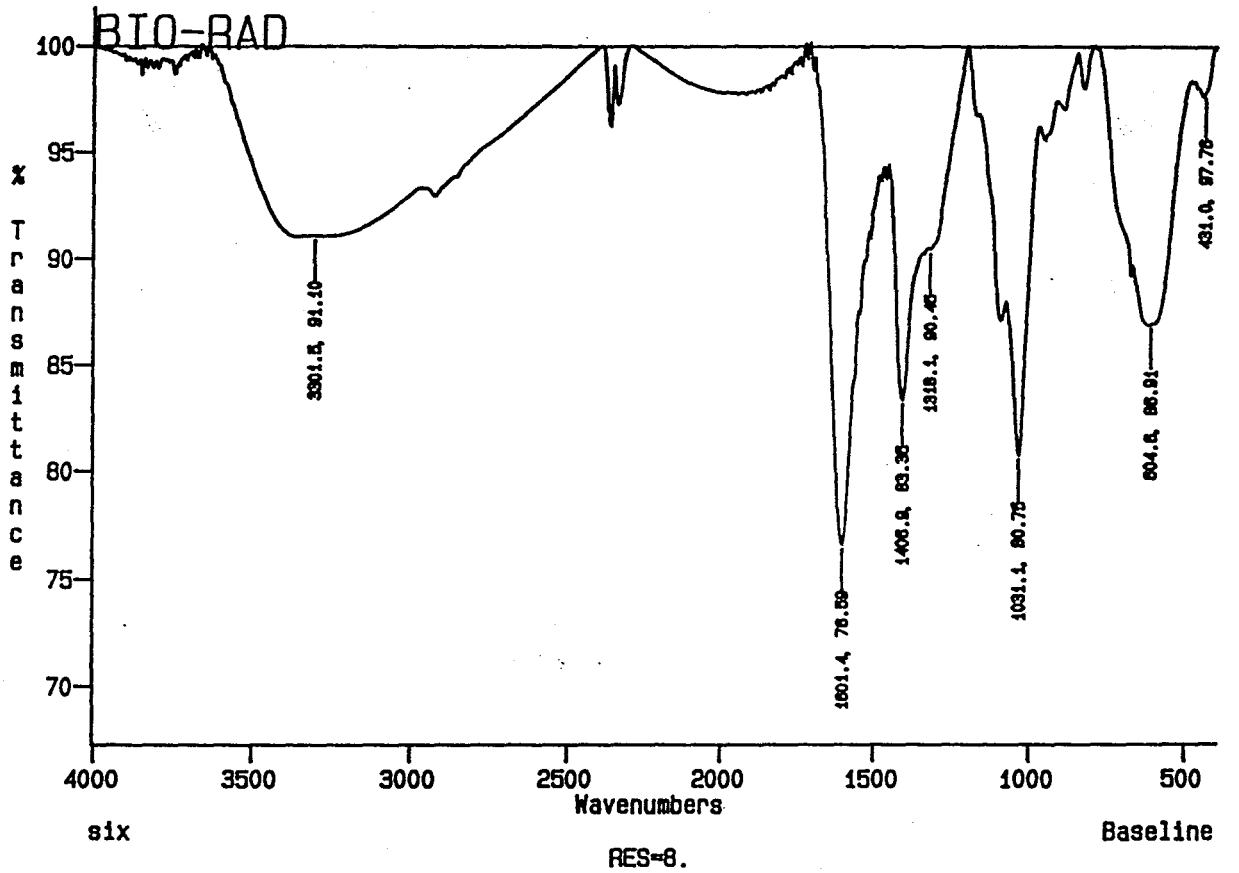

magnetite. Magnetite exhibits IR bands at 400 cm^{-1} and 590 cm^{-1}.[62]

Crystallographic Identification of Iron Oxide Particulates

Diffraction patterns of iron oxide containing alginate, generated by powder x-ray (Figure 23) and electron diffraction (Figure 24), narrowed the identity of the product oxide to two species: maghemite (spinel γ-Fe_2O_3) and/or magnetite (inverse-spinel Fe_3O_4). The calculated and measured d-spacing values from both diffraction patterns are summarized in Table 3. Table 4 lists the crystal class and characteristic d-spacing values associated with the oxide and oxyhydroxide products shown in Figure 5. A complete table of iron oxide and oxyhydroxide d-spacing values with corresponding (h,k,l) Miller indices is provided in Appendix 3.

Table 3. Experimental d-Spacing Values from Iron Oxide Alginate Diffraction Patterns.

***d* measured[1](Å)** (TEM) Electron Diffraction of Fourth Loaded Ferrofluid (120keV)	***d* calculated[2](Å)** Powder Xray Diffraction of Fifth Loaded Iron Oxide Alginate
2.93	2.97
2.50*	2.52*
2.07	2.10
1.60	1.61
1.45	1.47

1 Radius of rings, generated by selected area electron diffraction, were measured on-line and averaged over five areas of the specimen.
2 Calculated from powder diffraction pattern and Bragg's Law.
* Most intense diffraction ring and peak.

Figure 23. Powder x-ray diffraction pattern of sixth loaded iron oxide alginate (top) with the reference diffraction patterns of maghemite and magnetite.

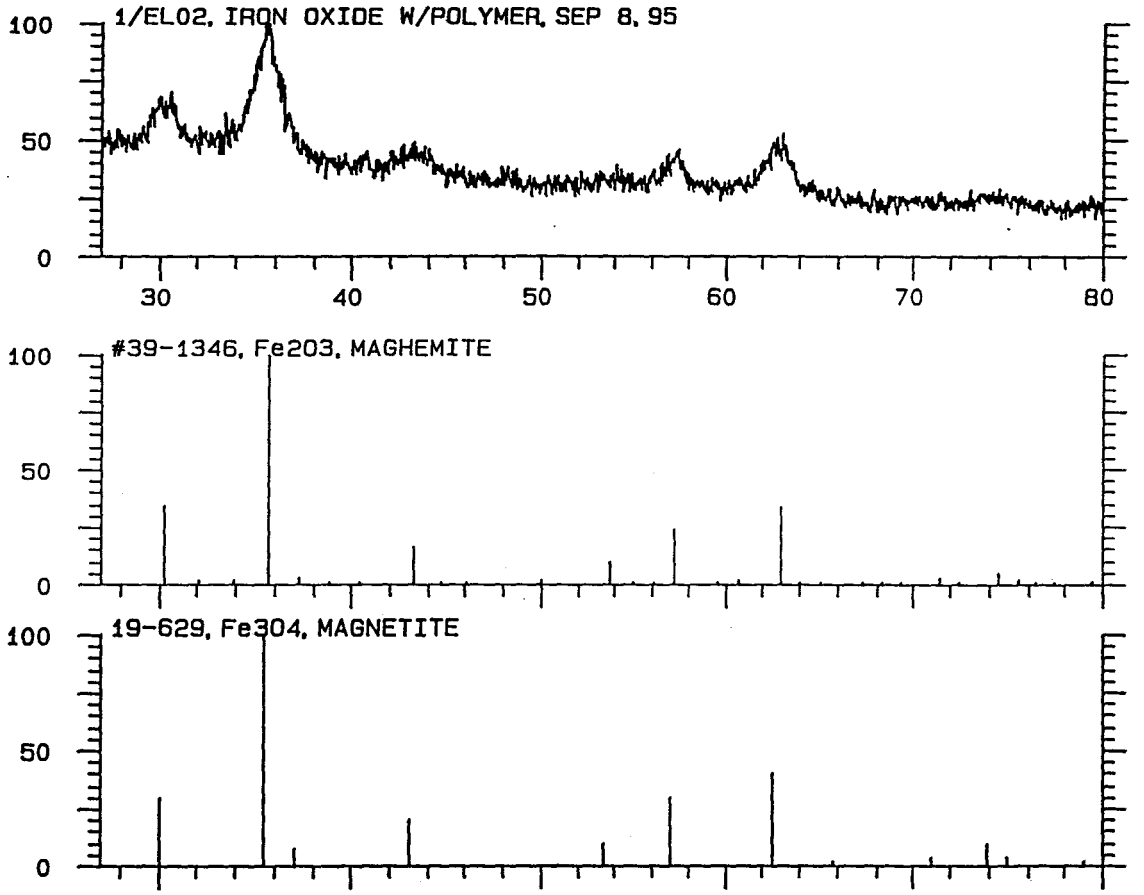

Figure 24. Selected-area electron diffraction pattern of dehydrated magnetic fluid prepared from fourth loaded iron oxide alginate gels (120keV, camera length 530mm).

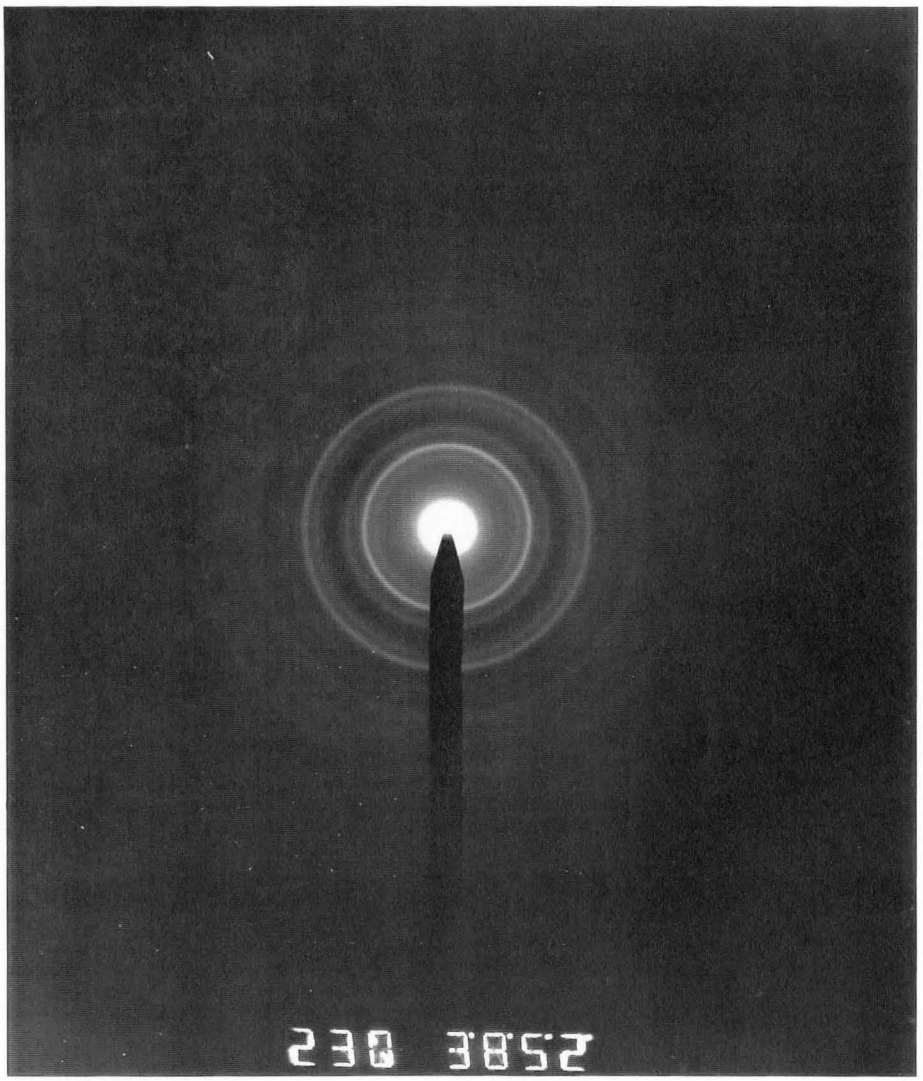

Table 4. Characteristic d-Spacing (Å) Values for Iron Oxides and Oxyhydroxides[63] (See Appendix 3 for corresponding Miller (h,k,l) indices)

Magnetite Fe_3O_4 Cubic	**Maghemite** γ-Fe_2O_3 Cubic	**Hematite** α-Fe_2O_3 Trigonal	**Geothite** α-FeOOH Orthorhombic	**Lepido-crocite** γ-FeOOH Orthorhombic	**Feroxyhyte** δ'-FeOOH Hexagonal
2.97	**2.95**	**2.69***	3.00	**6.26***	**0.254**
2.53*	**2.52***	**2.51**	**2.56**	**3.29**	0.222
2.42	2.08	2.20	2.25	2.79	0.169
2.10	1.61	2.07	1.95	**2.47**	0.147
1.71	**1.48**	1.69	**1.83**	2.36	
1.62	1.43	1.63	1.73	2.09	
1.49		1.59	**1.50**	**1.94**	
1.42		1.45			

Bold values represent characteristic d-spacing values for the crystal. Values with '*' are the most intense diffraction signals.

The most intense d-spacing values of pure and bulk phase maghemite and magnetite are very similar. Diffuse peaks and ring patterns, resulting from the distribution of size and orientation of fine grain crystalline samples, make it difficult to establish, with certainty, the identity of the precipitated iron oxide as pure γ-Fe_2O or Fe_3O_4, using the above diffraction techniques. In addition, diffracting impurities and astigmatism arising from interaction between the electron source and the magnetic sample contribute to broad diffraction signals.

Other results suggest that the predominant phase of iron oxide in the alginate gels, if a mixture of oxides does exist, is γ-Fe_2O_3. Color, for example, is a distinguishing feature of the different iron oxide and oxyhydroxide minerals. Magnetite is black while

maghemite is red-brown in color. Twice through sixth loaded iron oxide - alginate hydrogel beads appear dark brown in color. However, when a gel bead is pressed between two glass slides, the material is orange-brown.

Thermal analysis can be used to monitor the crystal structure transformations of iron oxide minerals which occur over specific temperature ranges. The following equation summarizes the temperatures and transformations of magnetite and maghemite:

$$Fe_3O_4 \xrightarrow{275\text{-}371\,^\circ C} \gamma\text{-}Fe_2O_3 \xrightarrow{500\text{-}700\,^\circ C} \alpha\text{-}Fe_2O_3$$

Both transformations are exothermic. TGA/DTA curves of sodium alginate and sixth loaded iron oxide alginate are shown in Figure 25. The product recovered from thermal treatment of the iron oxide sample was identified as hematite by powder x-ray diffraction The exotherm at 220°C in both samples corresponds to the decomposition of alginate which loses 40% of its inital weight by 250°C. The loss of adsorbed water associated with the polymer and the metal oxide and dehydroxylation occurs over the temperature range 220°C to 400°C. The broad exotherm from 500-1000°C could correspond to the transformation of γ-Fe_2O_3 to α-Fe_2O_3 ; however, possible interaction between the oxide and products of alginate combustion complicate interpretation of the TGA/DTA curve . The exothermic transformation of Fe_3O_4 to γ-Fe_2O_3 is not evident in the DTA curve.

The formation of γ-Fe_2O_3 from aqueous Fe^{2+} typically occurs at temperatures higher than 60°C. Fe^{2+}-crosslinked beads in methanol-water are stable at T>80°C but

Figure 25. Thermal gravimetric and differential thermal analysis curves of solid sodium alginate (top) and dehydrated sixth loaded iron oxide- alginate composite (bottom).

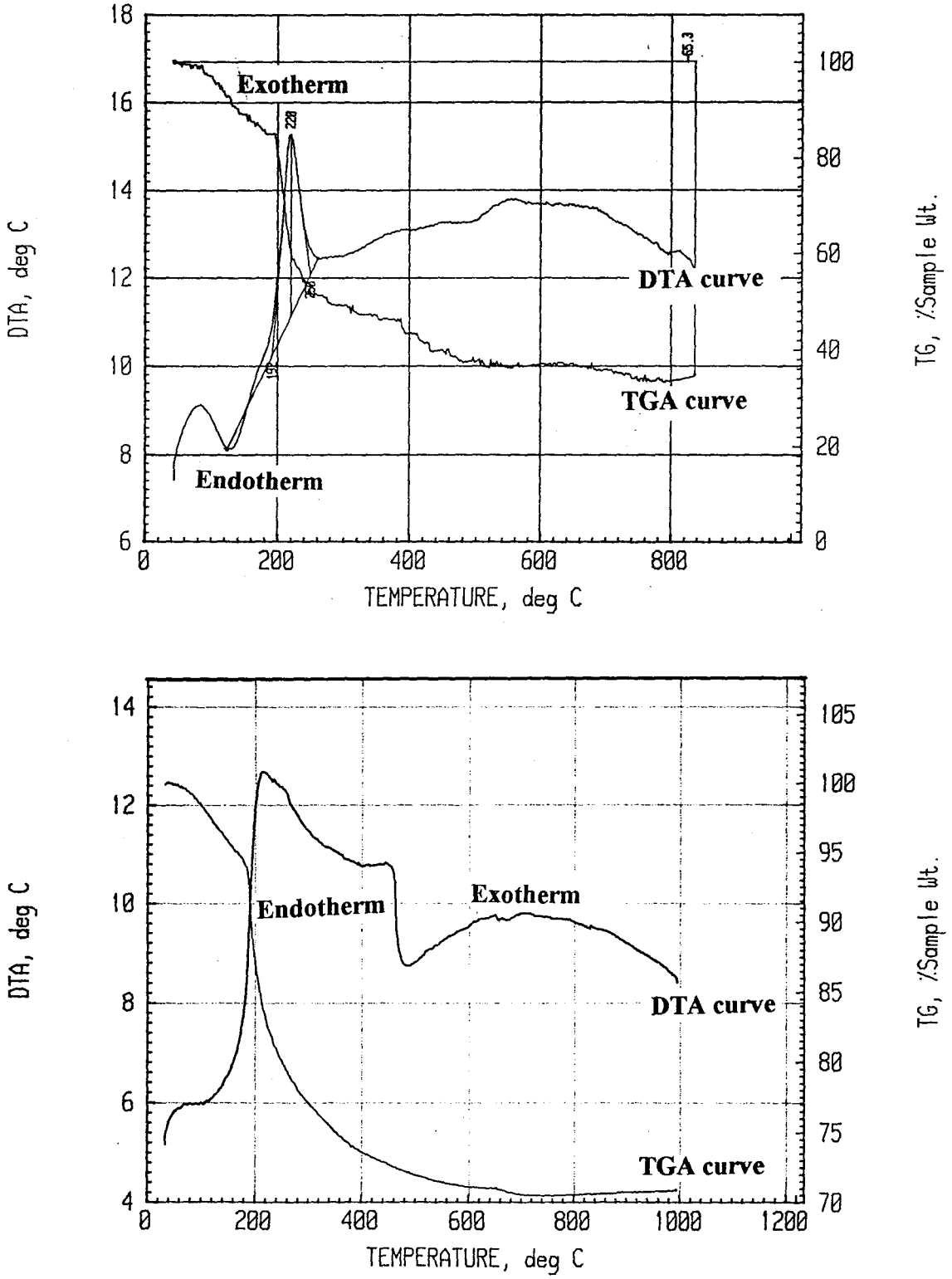

degrade at temperatures as low as 40°C when OH- is added. Because of this, base hydrolysis (pH 14) and oxidation of Fe^{2+}-alginate and iron oxide containing beads were performed at room temperature. The formation of maghemite as room temperature is unusual. Studies have shown, however, that maghemite can be precipitated from aqueous Fe^{2+} at pH 6-7, or without base, at elevated temperatures, as shown in Fig.5, Eq. 7. These reaction conditions were attempted with Fe^{2+}-crosslinked beads. The formation of maghemite, or other oxide product, at neutral pH was not observed with Fe^{2+}-crosslinked alginate under reflux at 75°C. Unlike the precipitation of iron oxides from bulk solution, the mechanism of nucleation of ions and crystal growth is different when iron cations are bound to a matrix.

Magnetic Properties of Iron-Oxide Alginate Composites

Iron oxide alginate gels are superparamagnetic at room temperature. First loaded alginate gels are weakly magnetic while superparamagnetic behavior is macroscopically observable for the higher loaded gel samples. Magnetic strength increased with the weight percent of iron in the gel. Magnetic contributions from alginate, which is diamagnetic, are negligible. Saturation magnetizations of iron oxide-alginate are calculated from the measured component of magnetization at maximum applied field strength and the known weight of the composite. The %Fe (w/w) and saturation magnetizations at 30kOe and 300K of dehydrated iron oxide-alginate gels (1-6 loadings) are summarized in Table 5.

Table 5. Magnetic Properties of Iron Oxide Alginate Beads[1]

Loading	Avg. %Fe (w/w)	Saturation Magnetization at 30kOe, 300K (emu/g material)
1	14.12	1.13
2	28.04	8.11
3	36.00	16.60
4	40.50	20.32
5	45.94	21.51
6	50.29	23.27

1 Data collected from one batch of 1-6 loadings

Magnetization curves of iron oxide-alginate are shown in Figure 26. At ambient temperatures, the magnetization curve lacks hysteresis with zero coercivity and remanence. The saturation magnetization of alginate taken through six reaction cycles is ~24 emu g^{-1} of composite. When the temperature of the system is lowered to 5K, the ferromagnetic properties of the iron oxide are recovered. At zero field, residual magnetization in the material is 7.8 emu g^{-1}. Coercivity, or the amount of applied field required to reduce the net magnetization of the composite to the lowest value (0.002emu), is 600 Oe. The above general features of superparamagnetism were observed for all iron-oxide containing alginate samples.

Magnetization curves of sixth loaded iron-oxide alginate composite at 30kOe were measured at 5K, 25K, 35K, 50K and 300K . As expected, the saturation magnetization

Figure 26. Magnetization curves of sixth loaded iron oxide-alginate: superparamagnetic at 300K (top) and ferromagnetic at 5K (bottom).

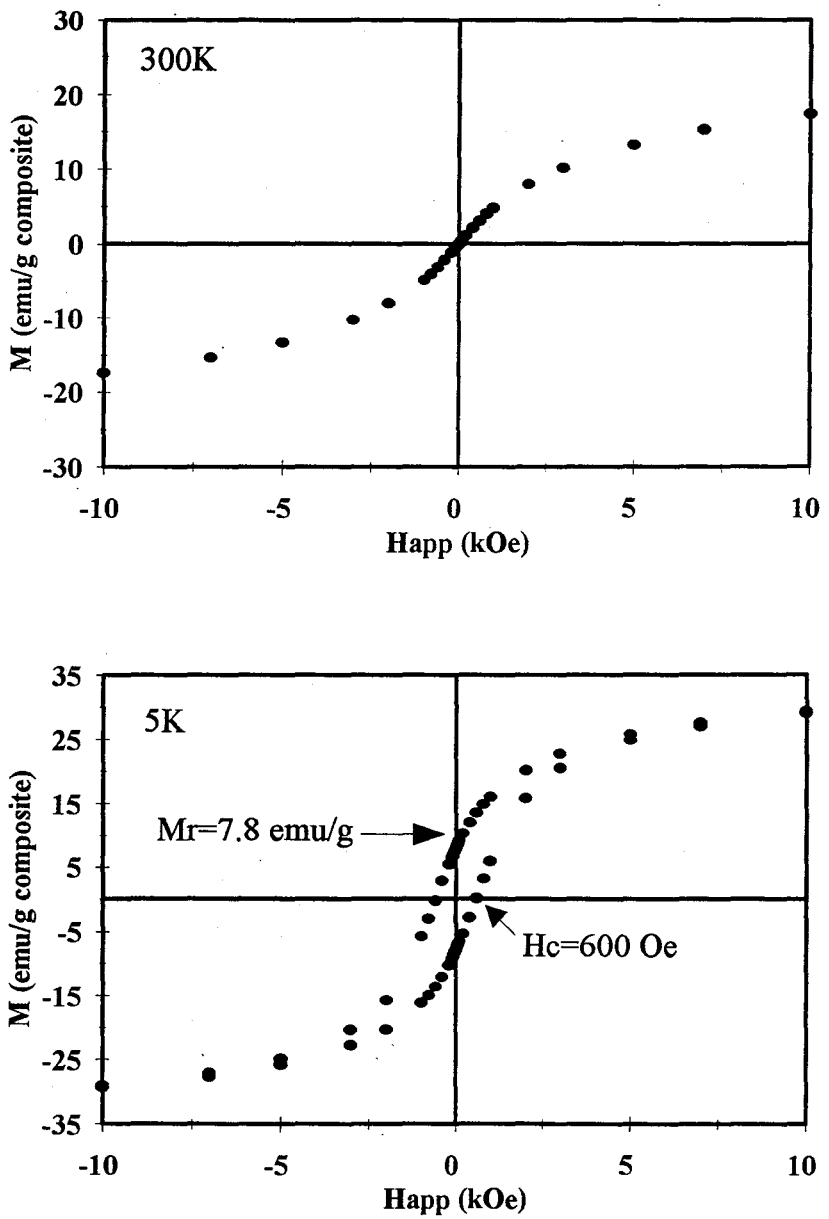

of the composite increased as the temperature of the system was lowered and the spin disordering effects of thermal agitation were repressed. Magnetization curves at different temperatures plotted against H/T are shown in Figure 27. At temperatures above 50K, superparamagnetic properties are observed and the magnetization curves superimpose. Below 50K, the magnetization traces of the composite exhibit weak hysteresis. The blocking temperature of the composite, or the transition temperature between superparamagnetism and ferromagnetism, can be estimated from a plot of the remanence of the material at zero applied field as a function of temperature (Figure 28). The blocking temperature for the iron oxide alginate composite is estimated to lie between 35K and 25K, where the magnitude of remanence increases sharply.

Figure 27. Magnetization curves of sixth loaded alginate at T≥ 50K are single-valued and superimpose at the origin unlike the ferromagnetic curve at 5K.

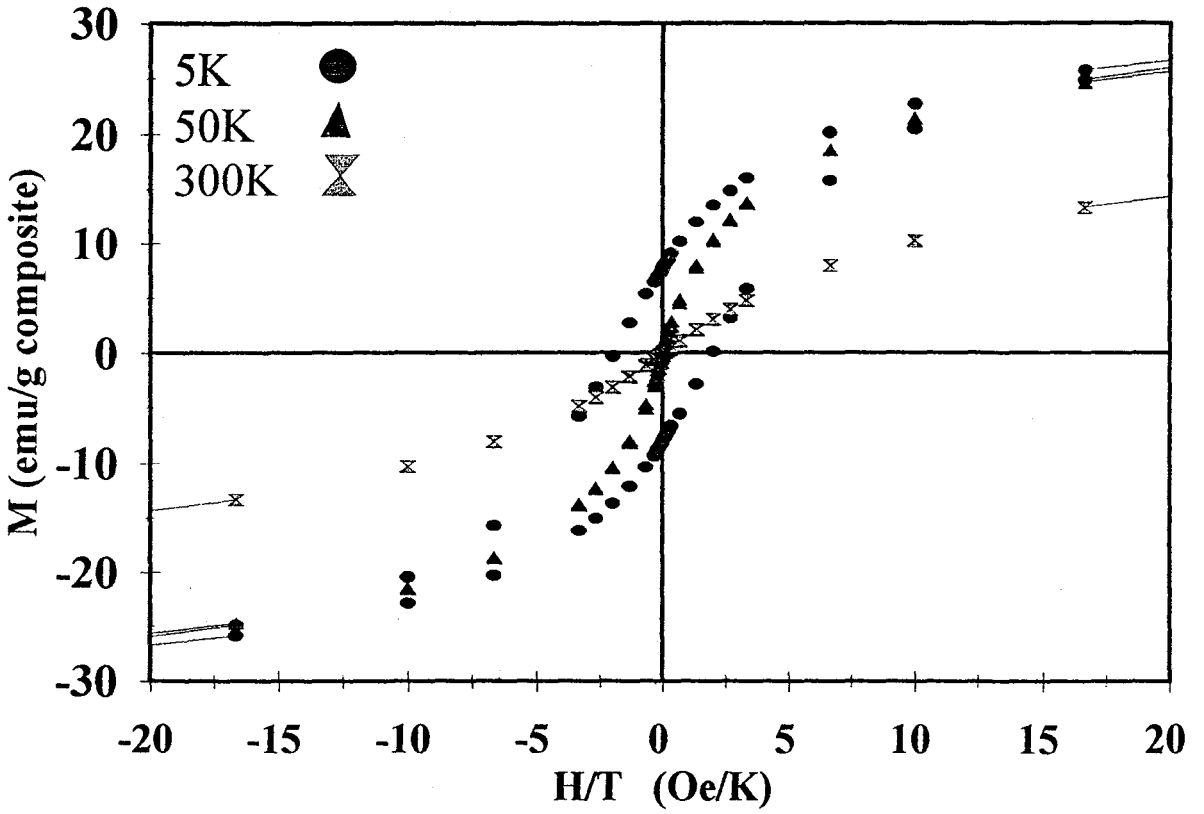

Figure 28. The magnitude of remanence for sixth loaded iron oxide alginate is temperature-dependent. Zero remanence is characteristic of superparamagnetic materials.

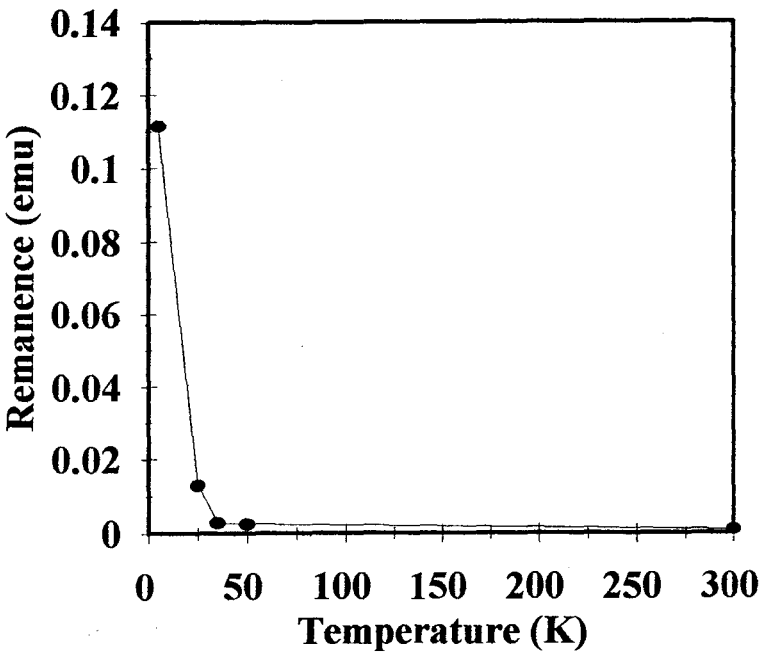

At 300K, the saturation magnetization of bulk phase γ-Fe_2O_3 and Fe_3O_4 are 76 emu g^{-1} and 90 emu g^{-1}, respectively. The saturation magnetization of nanocrystalline iron oxides is typically 10-15% less than the bulk values.[64] In addition to size and shape anisotropies, the existence of a 'magnetic dead layer', or the canted arrangement of spins in the surface layers of the single domain particle is proposed to contribute to decreased values of magnetization of nanocrystalline oxides compared to bulk phase oxides. For sixth loaded iron oxide-alginate, the measured saturation magnetizations are 30-36%

lower than the magnetizations for pure, bulk phase Fe_3O_4 and γ-Fe_2O_3. The additional difference in magnetization of iron oxide alginate may be due to: water adsorbed to the surface of the oxide particle, the size distribution of iron oxide particluates in the alginate matrix, or differing magnetic contributions from mixed iron oxides.

Oxide Particle Morphology within Gels

TEM bright-field images of sectioned alginate-iron oxide revealed the relative size, shape and distribution of iron oxide particulates in the composite. Photomicrographs of twice-(200 kX) and sixth- loaded gels (105 kX) are shown in Figures 29 and 30, respectively. The crystalline oxide particles appear both as isolated and existing in clusters. Clusters may exist as a consequence of loading, specimen preparation, and/or two dimensional particle imaging overlap. Isolated particulates are roughly spherical and range in diameter from 3-6 nanometers. Clusters have approximated diameters between 10-31 nanometers.

The three dimensional network of Fe^{2+}-crosslinked alginate is not regular but will have regions of crosslinked junction zones with interspersed regions of uncomplexed alginate. At lower magnification (Fig. 30), the iron oxide particles are not evenly distributed throughout the matrix but are concentrated along narrow linear regions or 'chains'. These regions may correspond to the interchain junction zones of alginate G blocks where crosslinking and iron oxide crystal growth occurred.

Figure 29. TEM photomicrograph of twice-loaded iron oxide alginate gel bead. Dark areas are the iron oxide nanocrystals (50keV, 200kX).

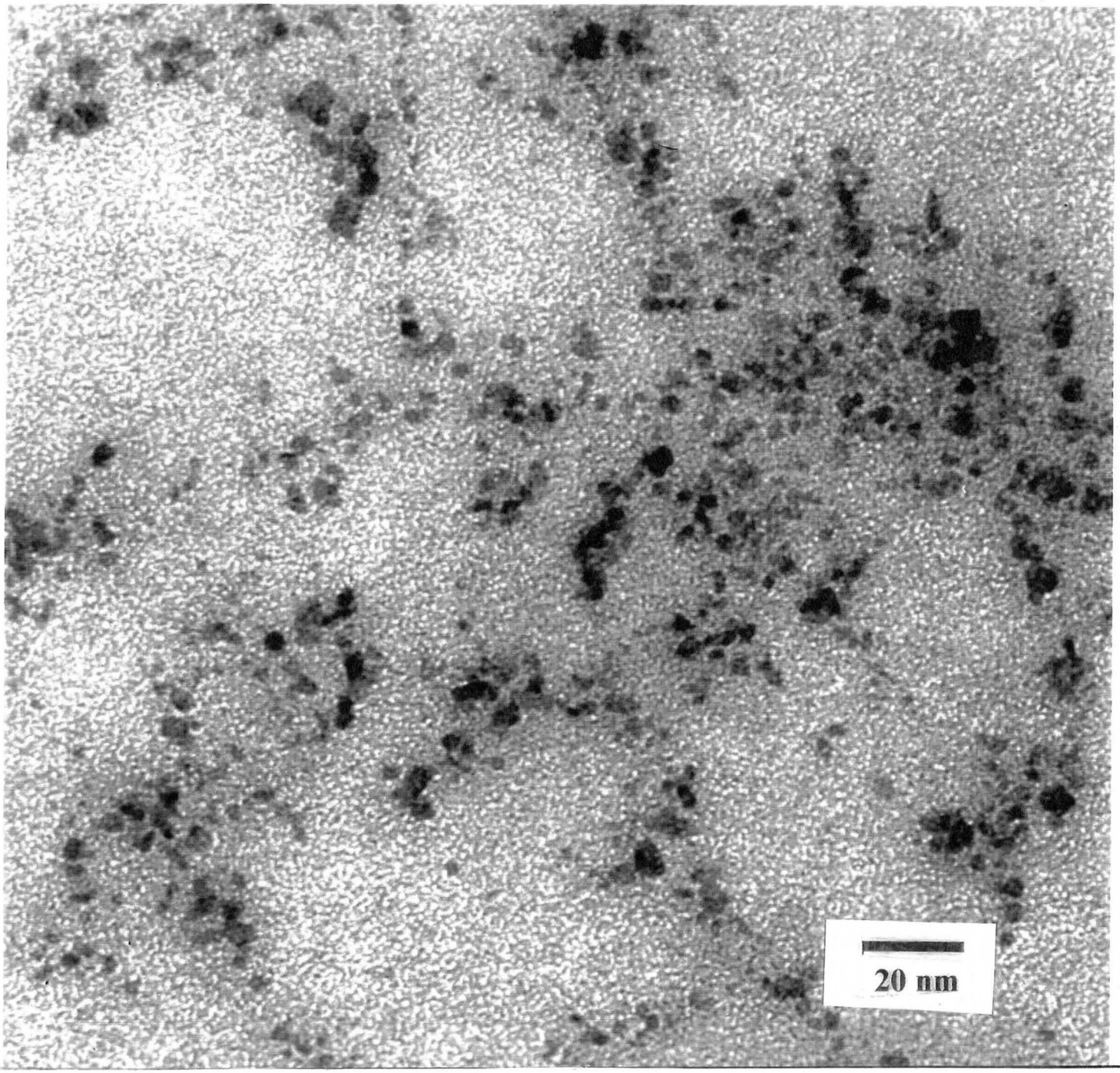

Figure 30. TEM photomicrograph of sixth-loaded iron oxide alginate gel bead. At lower magnification, the iron oxide particles appear to be agglomerated along 'chains' as opposed to being evenly dispersed throughout the alginate gel matrix (50keV, 105kX).

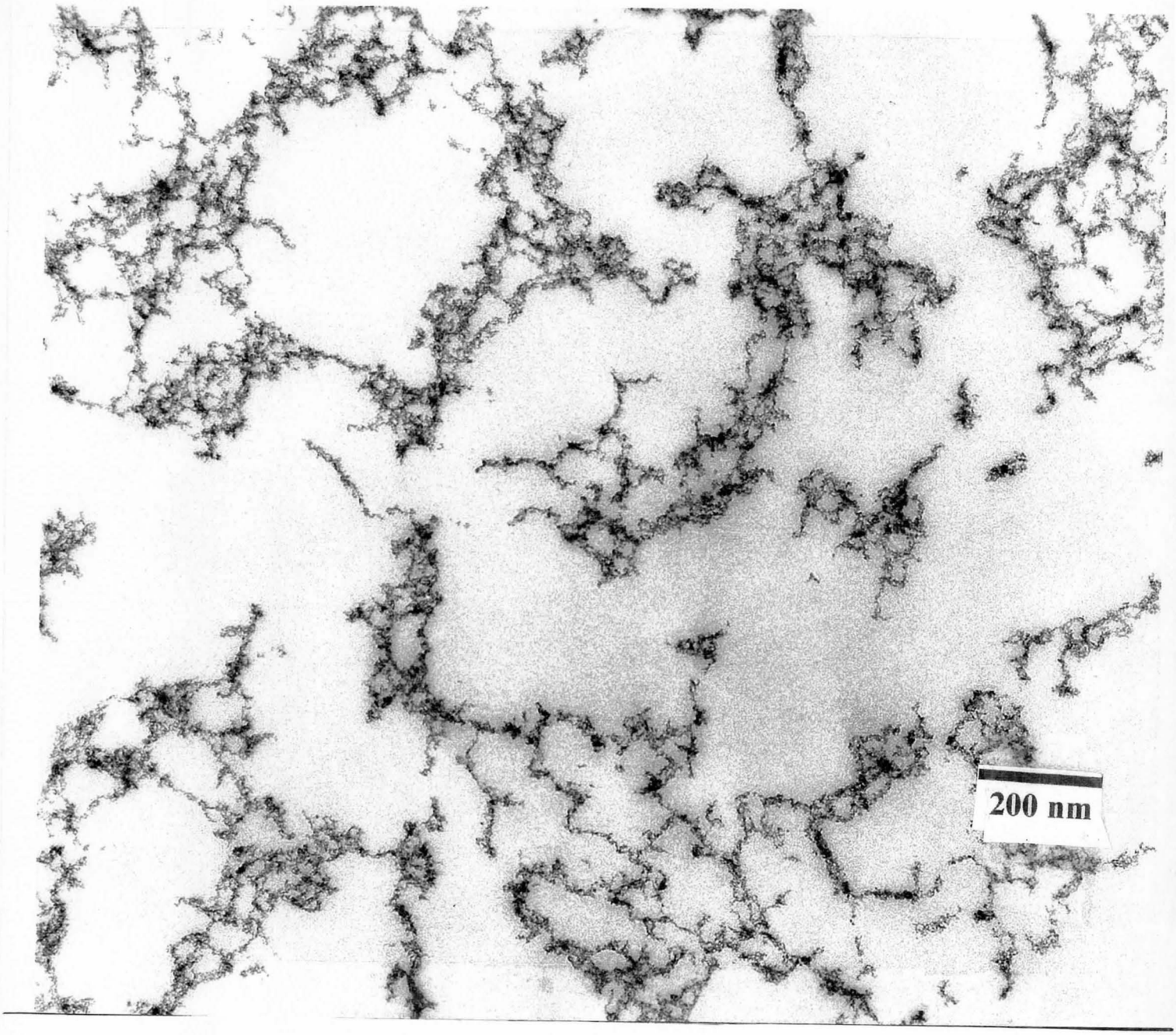

Template Effects on Oxide Particle Morphology

To date, the synthesis of gel phase magnetic nanocomposites has been limited to entrapment of pre-formed nanocrystalline iron oxides or magnetic sols within gels. Generally, this is accomplished by crosslinking a polymer in the presence of the oxide or sol. Magnetic alginate, for instance, has been prepared by entrapping small particles of iron oxide into a Ca^{2+}-crosslinked gel matrix.[65] The approach described here is unique in that the crosslinking agent, Fe^{2+}, is also the precursor of oxide formation. The structural integrity of the gel, as a function of G block concentration and crosslinking by iron, and the morphology of the nanoparticles are interdependent. Unlike rigid matrices, such as divinyl benzene crosslinked ion exchange resins, alginate hydrogels are flexible. Differences in the structural confinement and concentration of reaction sites are correlated with the irregular shape and size distribution of crystalline particles in alginate beads in comparison to the spherical and narrow size range observed in the exchange resins having regular pore sizes. Likewise, the high concentration of acicular ferrites, of varying length, aggregated at the surface of cellulosic fibers has been attributed to the large lumen or reaction volume of the raw or modified material.[66]

4.4. Iron Oxide-Alginate Hydrogel Derived Magnetic Fluid

Superparamagnetic water-based magnetic fluids were prepared from sixth-loaded iron oxide alginate hydrogels by a combination of physical and chemical degradation of the gel matrix. First, methanol, used to inhibit depolymerization of alginate during the

reaction of alginate with iron, sodium hydroxide, and oxygen, is removed from the magnetic beads. Iron crosslinked and iron oxide containing alginate beads swell and dissolve in water, however, complete disintegration of the gel structure by this method requires two to four days. Sonication accelerates the physical degradation of the gel matrix , which liquifies the gel within thirty minutes. A known promoter of the oxidative-reduction depolymerization reaction, either citrate or sodium phosphate, is added to assist in chemical degradation of alginate.

After dissolution of the magnetic gel, the fluid is purified. High molecular weight iron oxide-alginate aggregates, approximately 3% (w/w) solid material, are removed from the fluid by centrifugation. The fluid is then concentrated using ultrafiltration which removes water and low molecular weight alginate fragments (MW< 30,000 Daltons). Alginate was identified in solids recovered from the colorless filtrant by FTIR. The resulting liquid is a orange-brown in color, free of solids, optically transparent, and superparamagnetic.

The aqueous ferrofluid is composed of alginate-stabilized magnetic iron oxide particles. The Fe: polymer ratio of the liquid is 1.136 g Fe: g polymer, which is ~10% higher than that of the iron oxide gel precursor. When dehydrated, the saturation magnetization of the ferrofluid is 19.1 emu g^{-1} at room temperature and 30kOe. The iron oxide particles of the ferrofluid, examined by TEM of dehydrated ferrofluid, are isolated and spherical with diameters ranging between 4nm and 5.5nm. The effective diameter of the colloid is 54 nm in water and increases to 118nm in 0.01M NaCl and to 128nm in

0.1M NaCl.

The FTIR spectrum of dehydrated ferrofluid is similar to that of the sixth loaded iron oxide alginate gel precusor. As mentioned earlier, strong bands associated with Fe-O stretching and O-Fe-O deformations in the spectrum of sixth loaded gels, also appear in the spectrum of dehydrated ferrofluid (Figure 31). Also, the -OH stretching band remains shifted to lower frequencies. Physico-chemical properties of the magnetic fluid are summarized in Table 6.

Table 6. Properties of Magnetic Fluid prepared from Sixth Loaded Iron Oxide Alginate Hydrogel Beads

% Solids ((w/w)Alg and iron oxide)	5.8%
% Fe (w/w) in the solids	53.2%
Iron Oxide Particle Diameter	4.0-5.5 nm
Diameter of Colloid (H_2O)	54 nm
Polydispersity of Colloid	0.3661 ±10.53%
pH	6.8
pH zero point charge	2.75-2.8
Zeta Potential at pH 7 (30kV)	-51.6 mV

The pH of zero point charge for the water-based iron oxide alginate colloid, determined by titrating a dilute sample of the liquid with 0.01M HCl, is pH 2.75. The pHzpc of maghemite in water is pH 7.8 . The difference in pHzpc indicates chemical interaction between the iron oxide particles and the stabilizing polysaccharide. The pHzpc of the ferrofluid was marked by macroscopic flocculation of the suspended particles from

Figure 31. FTIR spectrum of freeze-dried ferrofluid prepared from sixth loaded iron oxide alginate gel beads.

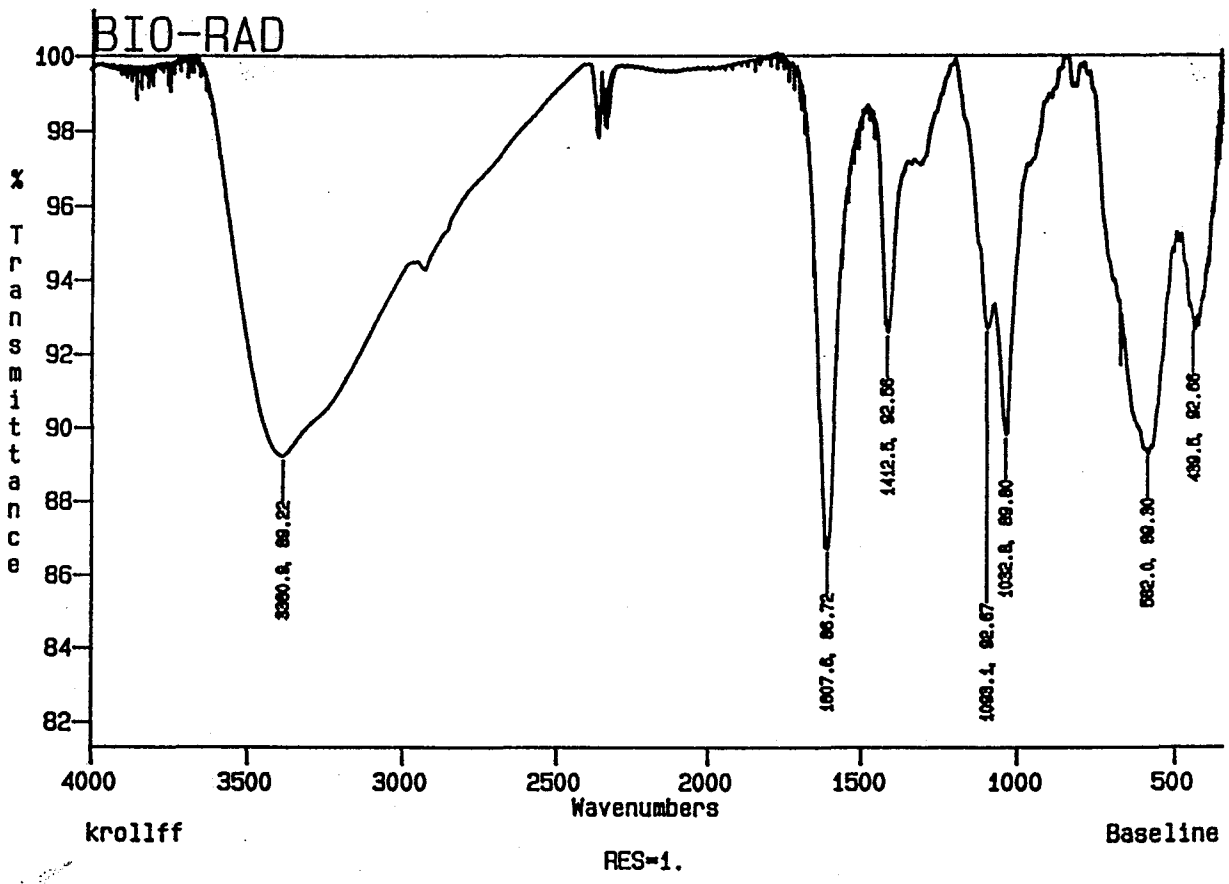

solution. The magnetic flocculate can be resuspended by adding base to form a stable dispersion. The colloidal suspension is stable at 2.8<pH<10. The ferrofluid is immiscible with alcohols.

Capillary electrophoresis was used to determine the effective charge density and purity of the ferrofluid. The electrophoretic mobility of the magnetic particles increases slightly with increased magnitude of applied electric field strength. Electrophoretic mobility does not vary significantly with changes in the pH of the sample (Figure 32). The colloid is negatively charged, arising from the polysaccharide stabilizing the magnetic core, with an average zeta potential of -51.6 ± 0.2mV.

Figure 32. Electrophoretic mobilities of alginate ferrofluid as a function of pH and applied voltage.

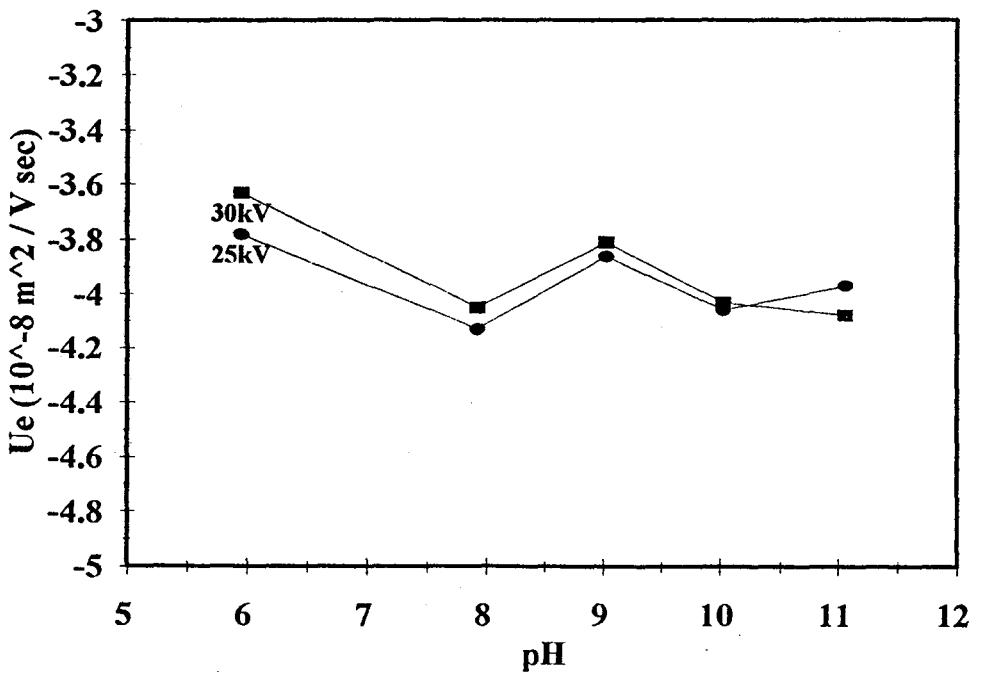

Capillary electrophoresis has been used to determine the relative purity of magnetic fluids.[67] The alginate ferrofluid is relatively free of unbound alginate, or impurities, as demonstrated by the CE generated electropherograms (Figure 33).

Figure 33. Electropherograms of alginate ferrofluid at 25kV and different pH: (I) pH 7.93, (II) pH 9.03, and (III) pH 10.03. (1mM phosphate buffer, UV detector, λ=254 nm).

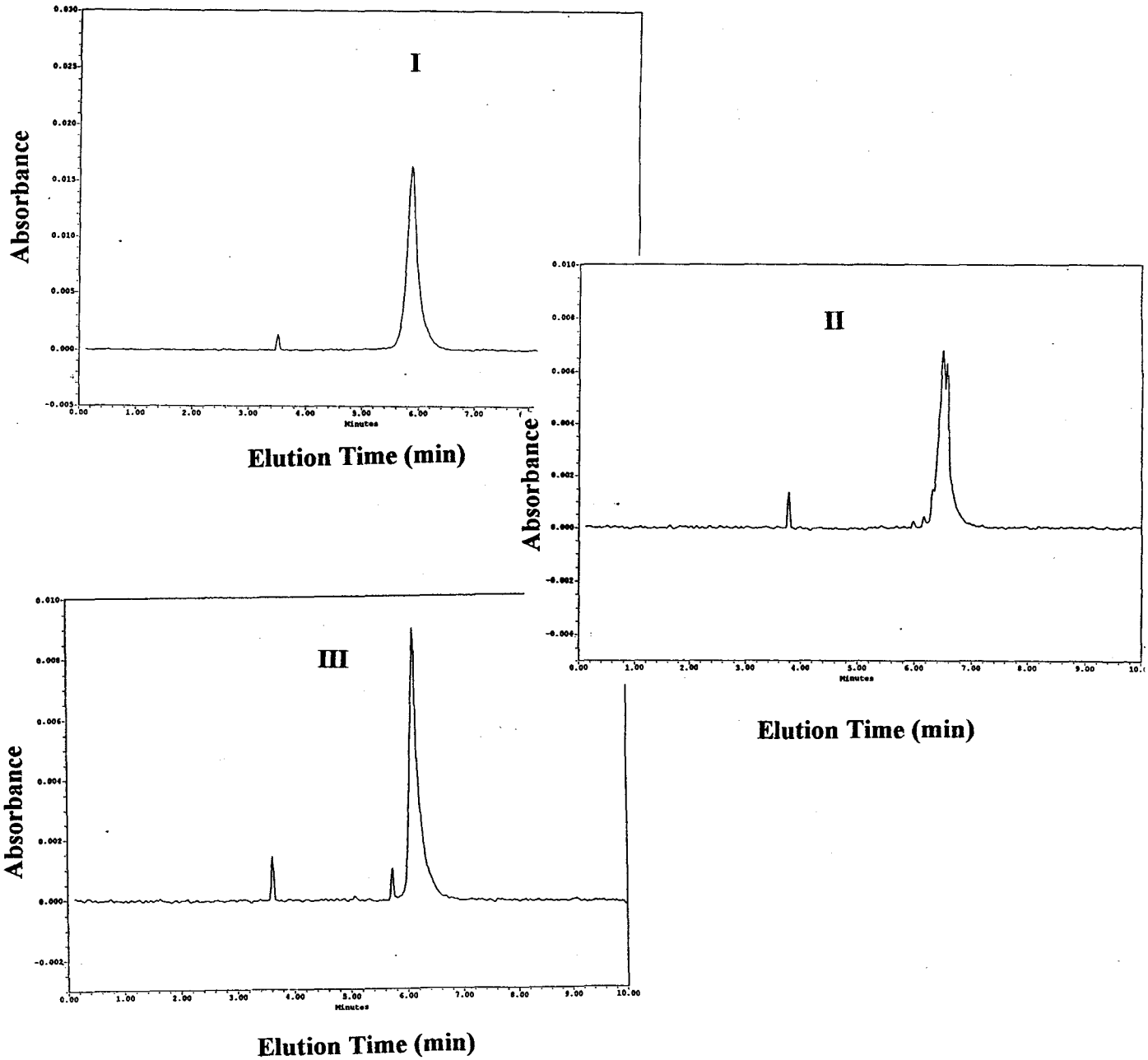

5. CONCLUSIONS AND RECOMMENDATIONS FOR FUTURE RESEARCH

The preparation of superparamagnetic iron oxide- alginate hydrogels and fluids is reproducible. The design and synthetic methodology is novel in two respects: 1) the gel-forming and depolymerization of alginate were used and controlled in the design and preparation of biocompatible superparamagnetic fluids; and 2) a stable magnetic fluid can be prepared from the hydrogel in less than two hours and without extreme chemical or physical methods such as attrition or heating.

In the 1930's, ferrous ions and oxygen were identified as the most notorious promoters of polysaccharide degradation. Fe^{2+}-crosslinked alginate hydrogels can be prepared in the presence of methanol, an inhibitor of alginate degradation. The precipitation of iron oxide into the gel matrix is possible only when uncomplexed ferrous ions are rinsed from the gels prior to base hydrolysis and oxidation and when methanol is present. As the concentration of iron oxide particles in the matrix increases, interaction between the iron oxide crystal and the polysaccharide matrix increases as evidenced by the volume reduction of the gel and from FTIR investigations. Once magnetic, the gel matrix is degraded by removing methanol. The addition of a depolymerization promoter and sonication are used only to accelerate the transformation. The resulting colloid consists of alginate-stabilized iron oxide nanocrystals. The low pHzpc of the fluid suggests interactions between the iron oxide particle surface and alginate.

The design and groundwork for the reproducible preparation and characterization of iron oxide- alginate magnetic gels and fluids were detailed in this thesis. Future work should be directed toward optimizing the preparation of strongly magnetic iron oxide hydrogels. This may include investigating alginates with a higher G block concentration and determining the optimal concentration of reagents (ie alginate, crosslinking solution, methanol, and sodium hydroxide). Also, the phase and concentration of the iron oxide(s) in the alginate matrix should be resolved using Mossbauer analysis then correlated with the preparative conditions.

6. APPENDICES

Appendix 1. Commercial applications of sodium alginate in food and industrial markets.

Food Applications of Alginates

Property	Product	Performance
Water holding	Frozen foods	Maintains texture during freeze–thaw cycle
	Pastry fillings	Produces smooth, soft texture and body
	Syrups	Suspends solids, controls pouring consistency
	Bakery icings	Counteracts stickiness and cracking
	Dry mixes	Quickly absorbs water or milk in reconstitution
	Meringues	Stabilizes meringue bodies
	Frozen desserts	Provides heat-shock protection, improved flavor release, and superior meltdown
	Relish	Stabilizes brine, allowing uniform filling
Gelling	Instant puddings	Produces firm pudding with excellent body and texture and better flavor release
	Cooked puddings	Stabilizes pudding system, firms body, and reduces weeping
	Chiffons	Provides tender gel body that stabilizes instant (cold makeup) chiffons
	Pie and pastry fillings	Acts as cold water gel base for instant bakery jellies and instant lemon pie fillings; develops soft gel body with broad temperature tolerance; gives improved flavor release
	Dessert gels	Produces clear, firm, quick-setting gels with hot or cold water
	Fabricated foods	Provides a unique binding system that gels rapidly under a wide range of conditions
Emulsifying	Salad dressings	Emulsifies and stabilizes various types
	Meat and flavor sauces	Emulsifies oil and suspends solids
Stabilizing	Beer	Maintains beer foam under adverse conditions
	Fruit juice	Stabilizes pulp in concentrates and finished drinks
	Fountain syrups, toppings	Suspends solids; produces uniform body
	Whipped toppings	Aids in developing overrun, stabilizes fat dispersion, and prevents freeze–thaw breakdown
	Sauces and gravies	Thickens and stabilizes for a broad range of applications
	Milk shakes	Controls overrun and provides smooth, creamy body

Painter, T. The Polysaccharides, Vol 2, ed. G. Aspinall, **1983**, Academic Press, NY, 449-457.

Appendix 1 (continued)

Industrial Applications of Alginates

Property	Product	Performance
Water holding	Paper coating	Controls rheology of coatings; prevents dilatancy at high shear
	Paper sizings	Improves surface properties, ink acceptance, and smoothness
	Adhesives	Controls penetration to improve adhesion and application
	Textile printing	Produces very fine line prints with good definition and excellent washout
	Textile dyeing	Prevents migration of dyestuffs in pad dyeing operations (algin is also compatible with most fiber-reactive dyes)
Gelling	Air freshener gel	Firm, stable gels are produced from cold water systems
	Explosives	Rubbery, elastic gels are formed by reaction with borates
	Toys	Safe, nontoxic materials are made for impressions
	Hydromulching	Holds mulch to inclined surfaces; promotes seed germination
	Boiler compounds	Produces soft, voluminous flocs easily separated from boiler water
Emulsifying	Polishes	Emulsifies oils and suspends solids
	Antifoams	Emulsifies and stabilizes various types
	Latexes	Stabilizes latex emulsions; provides viscosity
Stabilizing	Ceramics	Imparts plasticity and suspends solids
	Welding rods	Improves extrusion characteristics and green strength
	Cleaners	Suspends and stabilizes insoluble solids

Painter, T. The Polysaccharides, Vol 2, ed. G. Aspinall, **1983**, Academic Press, NY, 449-457.

Appendix 2. Colorimetric Quantification of Iron Using 1,10-Phenanthroline[57] in Magnetic Iron Oxide Alginate Hydrogels and Fluid.

Iron-crosslinked and iron-oxide alginate samples for iron quantification were freeze-dried after two rinses with water. A dry, powdered sample of known weight (1-5mg) was exposed to hydrochloric acid (12M, 2mL) for fifteen to twenty minutes. Acid digestion of the solid resulted in the extraction of iron from the polymeric material. The iron containing acid solution was filtered using a clean glass fritted funnel then transferred to a 10mL volumetric flask and diluted to mark with water. One milliliter of the dilute solution was transferred to a 25mL volumetric flask. To this, aqueous hydroxy ammonium chloride solution (BDH, 0.79M, 2.5mL), a reducing agent, was added to convert Fe^{3+} to Fe^{2+}. Next, aqueous 1,10-phenanthroline (Aldrich, 5.5mM, 5 mL) was added which forms a six coordinate, highly coloured complex with Fe^{2+}. The solution was diluted to mark with aqueous sodium acetate buffer (1.2 M, pH 3.5). The pH of the sample was monitored using a pH meter (Corning Digital pH Meter Model 320) and adjusted to pH 3.5 ± 0.01 with concentrated sodium hydroxide.

The calibration of iron concentration, using the 1, 10-phenanthroline colorimetric analysis, was performed by Dr. Andre Morneau. The absorption coefficient for complexed iron, $Fe(phen)_3$, was determined from the slope of absorption (λ=510 nm) as a function of iron concentration and has a measured value of 190.3 ± 0.8 [mole g^{-1} cm^{-1}] (R^2 = 0.9997)). Samples for iron quantification were analyzed in a quartz cell (l=1 cm)

using a Hewlett Packard 8452A Diode Array Spectrophotometer at 25C. Water was measured as background. The absorbance of complexed 1, 10- phenanthroline absorption was measured from 200 to 600 nm and the absorption at λ=510 nm was recorded for each sample. The following equations were used to determine the concentration, by weight, of iron in the original powdered sample:

Given:

Sample Mass (mg/10 mL of dilute HCl)	
Sample Volume (ml/25 mL)	
Absorbance (Absorbance Units)	

From Calibration:

Concentration of Fe (mg/ml)	(abs unit - 0.0081716/ 190.3013)
Conc Fe Stock (mg/ml stock)	(conc Fe)*25 / sample vol
Conc Fe t (mg/mass sample)	(Fe stock)*10

Calculated:

%Fe (w/w)	(conc Fe t/sample mass)*100
mole Fe (mol/mass)	(conc Fe t/1000)*55.85
mole Fe/g (mol/g)	(mole Fe/ (sample mass/1000))
$\%Fe_3O_4$ (w/w)	((moleFe/3)*231.537)/sample mass (g) *100
$\%Fe_2O_3$ (w/w)	((moleFe/2*159.691)/sample mass (g) *100

Appendix 3. Characteristic d-spacing values with associated (h,k,l) Miller indices for iron oxides and oxyhydroxides. [63]

Magnetite Fe_3O_4 Cubic	**Maghemite** γ-Fe_2O_3 Tetragonal	**Geothite*** α-FeOOH Orthorhombic	**Lepidocrocite** γ-FeOOH Orthorhombic	**Hematite** α-Fe_2O_3 Trigonal
2.97 (220)	**2.95 (206,220)**	4.98 (020)	**6.26*** (020)	**2.69*(104)**
2.53*(311)	**2.52* (119,313)**	**4.18* (110)**	**3.29 (120)**	**2.51** (110)
2.42 (222)	2.08 (400)	2.69 (130)	2.79 (011)	2.20 (113)
2.10 (400)	1.61 (513,339)	2.45 (111)	**2.47 (031)**	2.07 (202)
1.71 (422)	**1.48** (440)		2.36 (111)	1.69 (116)
1.62 (511)	1.43 (433,530)		2.09 (131,060)	1.63 (211)
1.49 (440)			**1.94** (051,200)	1.59 (018)
1.42 (531)				1.45 (300)

Bold values represent characteristic d-spacing values for the crystal. Values with '*' are the most intense diffraction signals.

* See also Mann, S; Hannington, J.P. *J. Coll. Interf. Sci.*,**1988**, 122(2), 330-336 .

7. REFERENCES

1. White, R.M. Materials Chemistry-An Emerging Discipline, Adv. in Chemistry Series 245, **1995**, ed. L.V. Interrante, L.A. Caspar, A.B. Ellis, ACS, Washington, DC, 5.

2. McMichail, R.D.; Shull, R.D.; Swartzendruer, L.J.; Bennett, L.H.; Watson, R.E. *J. Mag. Mag. Mater.*, **1992**, *111*, 29.

3. Chorney, A.F.; Mraz, W. *Machine Design*, May 7 **1992**, 79.

4. Atarashi, T.; Imai, T.; Shimoiizaka, J. *J. Mag. Mag. Mater.*, **1990**, *85*, 3.

5. Josephson, L.; Groman, E.V.; Menz, E.; Lewis, J.M.; Bengele, H. *Magn. Res. Imag.*, **1990**, *8*, 637.

6. Devineni, D.; Blanton, C.D.; Gallo, J.M. *Bioconj. Chem.* ,**1995** ,*6* , 203.

7. Standley, K.J. Oxide Magnetic Materials, 2nd ed., Claredon Press, Oxford, **1972**, 23-30.

8. Kittel,C. Introduction to Solid State Physics, 6th ed., John Wiley and Sons, NY, **1986**, 421-461.

9. Morrish, A.H. The Physical Principles of Magnetism, John Wiley and Sons, New York, 332.

10. Dunlop, D.J., *Physics of Earth and Planetary Interiors*, **1981,** *26*, 19.

11. Bean, C.P.; Livingston, J.D. *J. App. Phys.*, **1959**, *30(4)*, 120S.

12. Hurd, C.M. *Contemp. Phys.*, **1982**, *23(5)*, 469.

13. Berkowitz, A.E. Science and Techology of Nanostructructed Magnetic Materials, ed. G.C. Hadjipanayis and G.A. Prinz, Plenum Press, NY, **1991**, 533-544

14. Tronc, E.; Prene, P.; Jolivet, J.P.; d'Orazio, F.; Lucari, F.; Fiorani, D.; Godinho, M.; Charkaoui, R.; Nogues, M.; Dormann, J.L. *Hyperfine Inter.*, **1995**, *95*, 129.

15. Schwertmann, U.; Cornell, R.M. Iron Oxides in the Laboratory, VCH, NY, **1991**

16. Massart, R. *IEEE Trans. on Mag.*, **March 1981**, *17(2)*, 1247.

17. Bacri, J.C.; Perzynski, R.; Salin, D.; Cabuil, V.; Massart, R. *J. Mag. Mag. Mater.*, **1990**, *85*, 27.

18. Ziolo, R.F.; Giannelis, E.P.; Weinstein, B.A.; O'Horo, M.P.; Ganguly, B.N.; Mehorta, V.; Russel, M.W.; Huffman, D.R.; *Science*, **1992,** *257*, 219.

19. Pillai, V.; Kumar, P.; Hou, M.J.; Ayyub, P.; Shah, D.O. *Adv. Col. Int. Sci.*, **1995**, *55*, 241.

20. Kommareddi, N.S.; Tata, M.; John, V.T.; McPherson, G.L.; Herman, M.F.; Lee, Y.S.; O'Connor, C.J.; Akkara, J.A.; Kaplan, D.L. *Chem. Mater.*, **1994**.

21. Hamaya, T.; Takizawa, T.; Hidaka, H.; Horikoshi, K. *J. Chem. Eng Jap.* , **1993**, *26(2)*, 223.

22. Schiff, H.; Canal, G. *Bio. Cyb.*, **1993**, *69*, 7.

23. Kirschvink, J.L. *J. Exp. Bio.* , **1981**a, *92*, 333.

24. Meldrum, F.C.; Heywood, B.R.; Mann, S. *Science,* **1992**, *257*, 522.

25. Mann, S.;Hannington, J.P. *J. Col. Int. Sci.* , **1988**, *112(2)*, 326.;
Mann, S.; Hannington, J.P.; Williams, R.J.P. *Nature*, **1986**, *324*, 565.

26. Maruno,S.; Nasegawa, M. U.S. Pat. Publ. 5204457, **93/4/20**

27. Raymond. L.; Revol, J.F.; Ryan, D.H.; Marchessault, R. *Chem. Mater.*, **1994**, *6,* 249.

28. Molday, R.S.; Mackenzie, D. *J. Immun. Meth.*, **1982**, *52*, 353.

29. Wooding, A.; Kilner, M.; Lambrick, D.B. *J. Disp. Sci. Tech.*, **1992** *,13(5),* 479.

30. Thomas, T.E.; Abraham, S.J.R.; Otter, A.J.; Blackmore, E.W.; Lansdorp, P.M. *J. Imm. Meth.*, **1992**, *154*, 254.

31. Sandford, P.A.; Baird, J. The Polysaccharides, Vol II, ed. G Aspinall, Academic Press, NY, **1983**, 449-457.

32. Rees, D.A. *Biochem. J.*, **1972** ,*126*, 257.

33. Rees, D.A.; Morris, E.R.; Thom, D.; Madden, J.K. The Polysaccharides, Vol I, ed. G Aspinall, Academic Press, NY, **1982**, 222-233.

34. Percival, E.; McDowell, R.H. Chemistry and Enzymology of Marine Algal Polysaccharides, Academic Press, London, **1967,** 98-123.

35. Smidsrod, O. *Disc. Faraday Soc.*, **1974**,*57*, 263.

36. Smidsrod, O. *Carb. Res.*, **1973** , *27*, 32.

37. Smidsrod, O; Glover, R.M.; Whittington, S. *Carb. Res.*, **1973**, *27*, 107.

38. Smidsrod, O.; Haug, A.; Whittington, S. *Acta Chem. Scand.*, **1972**, *26(6)*, 2563.

39. Painter, T.J. The Polysaccharides, Vol II, ed. G Aspinall, Academic Press, NY, **1983**, 271-273.

40. Angyal, S.J. *Pure Appl. Chem.*, **1973**, *35*, 131.

41. Smidsrod, O.; Skjak-Braek,G. *TIBTECH*, **1990**, *8*, 71.

42. Martinsen, A.; Skjak-Braek, G.; Smidsrod, O.; *Biotech/Bioeng*, **1989**, *33*, 79.

43. Hofman, A.S.; Park, T.G. *J. Poly. Sci., Part A, Poly. Chem* , **1992**, *30*, 505.

44. Green, J.W.,The Carbohydrates, Vol 1B, ed W Pigman, D Horton, Academic Press, NY 1980, 1101-1133

45. Balazs, E.A.; Davies, J.V; Phillips, G.O.; Young, M.D. *Rad. Res.*, **1967**, *31*, 243.

46. Uchiyama, H.; Dobashi, Y.; Ohkouchi, K.; Nagasawa, K. *J. Bio. Chem.*, **1990**, *265(14)*, 7753.

47. Matsumura, G.; Herp,A.; Pigman, W. *Rad. Res.*, **1966**, *28*, 735.

48. Smidsrod, O.; Haug, A.; Larsen, B. *Acta Chem. Scand.*, **1963**, *17*, 2628.

49. Pigman,W.; Rizvi, S. *Biochem. Biophys. Res. Comm.*, **1959**, *1(1)*, 39.

50. Sundblad, L.; Balazs, E.A. Amino Sugars, Vol IIB, ed. E.A. Balazs and R.W. Jeanloz, 1966, Academic Press, NY, 229.

51. Smidsrod, O.; Haug, A.; Larsen, B. *Acta Chem. Scand.*, **1965**, *17*, 143.

52. Skjak-Braek, G.; Murano, E.; Paoletti, S. *Biotech. Bioeng.*, **1989**, *33*, 90.

53. Martinsen, A.; Skjak-Braek, G.; Smidsrod, O. *Biotech. Bioeng*, **1989**, *33*, 79.

54. Marchessault, R.H.; Rioux, P.; Raymond, L. *Polymer*, **1991**, *33*, 4025.

55. Penman, A.; Sanderson, G.R. *Carb.Res.*, **1972**, *25*, 273.

56. Grasdalen, H.; Larsen, B.; Smidsrod,O. *Carb. Res.*, **1979**, *68*, 23.

57. Saywell, L.G.; Cunnigham, B.B.; *Ind. Eng. Chem.*, **1936**, *9(2)*, 67.

58. Grasdalen, H.; Larsen, B.; Smidsrod, O. *Carb. Res.*, **1979**, *68*, 23.

59. Stumm, W. Aquatic Chemistry, ed. S.P. Huang, C.R. O'Melia, J.J. Morgan, American Chemical Society, **1995**, 2.

60. Tipson, R.S.; Parker, F.S. Carbohydrates: Chemistry and Biochemistry, 2 ed, Vol.1B, eds. W. Pigman and D. Horton, 1970, Academic Press, NY, 1398-1416

61. Jansen, E.F.; Jang, R. *J. Am.Chem.Soc.*, **1946**, *68*, 1475.

62. Taylor, R.M.; Schwertmann, U. *Clay Minerals*, **1974**, *10*, 299.

63. Selected Powder Diffraction Data for Minerals, Data Book, First Edition, Joint Committee on Powder Diffraction Standards, **1974**

64. Private Communication with Dr. R.F. Ziolo, Xerox Corporation, 2/10/1996

65. Hamaya, T.; Takizawa, T.; Hidaka, H.; Horikoshi, K. *J. Chem.Eng. Jap.*, **1993**, *26(2)*, 223.

66. Raymond, L.; Revol, J.F.; Marchessault, R.H. *Polymer*, **1995**, *36(26)*, 5035.

67. Morneau, A.; Winnik, F.M., Ziolo, R.F. Analysis of Ferrofluids by Capillary Electrophoresis (To be published)